Research paper

Optimal management of a hybrid and isolated microgrid in a random setting

Salvatore Vergine [a], César Álvarez-Arroyo [b], Guglielmo D'Amico [c], Juan Manuel Escaño [d,*], Lázaro Alvarado-Barrios [e]

[a] *Department of Neurosciences, Imaging and Clinical Sciences, University G. D'Annunzio, 66100 Chieti, Italy*
[b] *Department of Electrical Engineering, Universidad de Sevilla, 41092 Sevilla, Spain*
[c] *Department of Economics, University G. D'Annunzio, 65127 Pescara, Italy*
[d] *Department of Systems Engineering and Automatic Control, Universidad de Sevilla, 41092 Sevilla, Spain*
[e] *Engineering Department, Universidad Loyola Andalucía, Avda. de las Universidades s/n, 41704 Dos Hermanas, Spain*

ARTICLE INFO

ABSTRACT

Nowadays, governments and electricity companies are making efforts to increase the integration of renewable energy sources into grids and microgrids, thus reducing the carbon footprint and increasing social welfare. Therefore, one of the purposes of the microgrid is to distribute and exploit more zero emission sources. In this work, a Stochastic Unit Commitment of a hybrid and isolated microgrid is developed. The microgrid supplies power to satisfy the demand response by managing a photovoltaic plant, a wind turbine, a microturbine, a diesel generator and a battery storage system. The optimization problem aims to reduce the operating cost of the microgrid and is divided into three stages. In the first stage, the uncertainties of the wind and photovoltaic powers are modeled through Markov processes, and the demand power is predicted using an ARMA model. In the second stage, the stochastic unit commitment is solved by considering the system constraints, the renewable power production, and the predicted demand. In the last stage, the real-time operation of the microgrid is modeled, and the error in the demand forecast is calculated. At this point, the second optimization problem is solved to decide which generators must supply the demand variation to minimize the total cost. The results indicate that the stochastic models accurately simulate the production of renewable energy, which strongly influences the total cost paid by the microgrid. Wind production has a daily impact on total cost, whereas photovoltaic production has a smoother impact, shown in terms of general trend. A comparison study is also considered to emphasize the importance of correctly modeling the uncertainties of renewable power production in this context.

1. Introduction

1.1. Motivation

In recent years, there has been growing awareness among the world population of the need to demand that public administrations develop more sustainable economic development models for their countries (Pye et al., 2019). This requirement is justified by the growing demand for energy for domestic use and economic activities related to commerce, industry, and transport (Nejat et al., 2015), leading to an increase in greenhouse gas emissions and the depletion of fossil fuels (Gerbaulet et al.,

2019). As a consequence of these policies, electricity systems are making a transition from a centralized grid, composed of large and controllable power plants, transporting electricity over long distances and downstream, where the end user only consumes energy, to a decentralized grid based on the increased penetration of Distributed Energy Resources (DER), which integrates renewable energy sources (RES), electrical energy storage systems (EESS) and flexible demand side management (demand response, DR) (Kakran and Chanana, 2018), with the end user becoming an active element in the system (prosumer) (Rehman et al., 2019; REScoop.eu, 2020).

In this transition to a decarbonized energy model, microgrids play a key role, as they provide social, environmental, and economic benefits (Choudhury, 2022). They represent a local and sustainable energy supply that manages to integrate RESs such as photovoltaic (PV) and wind turbines (WT), controllable backup power sources such as diesel generators (DE) and microturbines

* Corresponding author.
E-mail addresses: salvatore.vergine@unich.it (S. Vergine),
cesaralvarez@us.es (C. Álvarez-Arroyo), g.damico@unich.it (G. D'Amico),
jescano@us.es (J.M. Escaño), lalvarado@uloyola.es (L. Alvarado-Barrios).

Acronyms

ARMA	Autoregressive Moving Average
BESS	Battery Energy Storage System
DE	Diesel Generator
DER	Distributed Energy Resource
DR	Demand Response
DSO	Distribution System Operator
ED	Economic Dispatch
EESS	Electrical Energy Storage Systems
EMS	Energy Management System
MT	Microturbine
NN	Neural Network
PV	Photovoltaic Unit
RES	Renewable Energy Source
SOC	State Of Charge
SUC	Stochastic Unit Commitment
TSO	Transmission System Operator
UC	Unit Commitment
WT	Wind Turbine
MINLP	Mixed Integer Nonlinear optimization Programming
MILP	Mixed Integer Linear optimization Programming
EABC	Extended Artificial Bee Colony Algorithm
MG	Microgrid
ILP	Integer Linear Programming
GA	Genetic Algorithm
PSO	Particle Swarm Optimization
AARO	Affinely Adjustable Robust Optimization
MCS	Monte Carlo Simulation
PDF	Probability Density Function
C&CG	Column and Constraint Generation
LCOE	Levelized Cost of Electricity
IGDT	Information Gap Decision Theory
HSS	Hydrogen Storage System

Parameters

a_i, b_i, c_i	Cost function coefficients of DE and MT
C_{MT}	Operation and maintenance cost of MT
C_{DE}	Operation and maintenance cost of DE
Δt	Time between samples
DE_{max}	Maximum generator capacity of DE
DE_{min}	Minimum generator capacity of DE
MT_{max}	Maximum generator capacity of MT
MT_{min}	Minimum generator capacity of MT
P^i_{max}	Maximum generation capacity of unit i
P^i_{min}	Minimum generation capacity of unit i
P^c_{max}	Maximum charging rate of the BESS
P^d_{max}	Maximum discharging rate of the BESS
SOC^i_{max}	Maximum state of charge of BESS i
SOC^i_{min}	Minimum state of charge of the BESS i
η_c	Battery charging efficiency
η_d	Battery discharging efficiency
E^{WT}	State space of WT power

E^{PV}	State space of PV power

Variables

$R^u_{DE}(t)$	Up spinning reserve of DE at time t
$R^d_{DE}(t)$	Down spinning reserve of DE at time t
$R^u_{MT}(t)$	Up spinning reserve of MT at time t
$R^d_{MT}(t)$	Down spinning reserve of MT at time t
$\omega(t)$	Power difference between actual and expected demand at time t
$\delta_{DE}(t)$	Power on/off variable of DE at time t
$\delta_{MT}(t)$	Power on/off variable of MT at time t
$B(t)$	Battery power at time t
$D(t)$	Power demand at time t
$\hat{D}(t)$	Power demand forecast at time t
$\hat{P}(t)$	Solar power forecast at time t
$\hat{W}(t)$	Wind power forecast at time t
$\hat{SOC}(j|t)$	Prediction of SOC for time j at time t
$DE(t)$	Power given by DE at time t
$MT(t)$	Power given by MT at time t
$PV(t)$	Power given by PV at time t
$WT(t)$	Power given by WT at time t
$R_{DE}(t)$	Power spinning reserve of DE at time t
$R_{MT}(t)$	Power spinning reserve of MT at time t
$SOC(t)$	State of charge of BESS i at time t
$SOC(t)$	State of charge of BESS i at time t
$SOC(t)$	State of charge of BESS i at time t
$SOC(t)$	State of charge of BESS i at time t
J^{WT}_n	WT-Markov chain
J^{PV}_n	PV-Markov chain
$\phi(s, t)$	Transition probability function
$P(k)$	non-homogeneous transition probability matrix
P	homogeneous transition probability matrix

(MT), EESSs and controllable loads (Xie et al., 2021). They can help integrate the above components into the grid, improving their reliability and reducing the dependence on fossil fuels that emit carbon for power generation (Trivedi et al., 2022). Current decentralization and co-ownership of the consumer in RESs require that these electricity systems support the growing penetration of electric vehicles, facilitate demand flexibility, enhance the active role of the consumer, and participate in the supply of complementary services to the distribution grid (Eghbali et al., 2022). For this reason, MGs face two major challenges in the future: on the one hand, overcoming the regulatory barriers that currently exist and, on the other hand, developing energy management tools that enable their optimal operation, whether connected to the main grid or in stand-alone mode, facilitating the interaction between electricity end-users and energy resource managers, transmission system operators (TSOs), distribution system operators (DSO) and the market operator.

1.2. Related work

Energy Management Systems (EMS) are an important part of the control of MGs. They allow monitoring, analyzing, and forecasting the power generation of RESs and demand, considering weather factors and prices of the energy market (Bordons et al., 2020). They also perform optimal short-term energy scheduling

of the MG, based on RESs forecasts and load demand, taking into account technical, economic and environmental aspects (Eghbali et al., 2022), as well as managing DER power flows in the MG, between it and the main grid, and among other MGs, and facilitating a smooth transition of MG operation modes, isolated and interconnected to the grid (Chen et al., 2011a). From the review of the literature, it can be seen that several optimization strategies or techniques have been proposed for EMSs applied to MGs (Zia et al., 2018). As MGs consolidate in the new energy model, as an important resource to increase the efficiency of DG systems and favor a greater penetration of RESs, the scientific literature shows an increase in approaches based on the resolution of the UC problem, as a basic tool in predictive planning of the operation of these systems (Moretti et al., 2020).

The UC problem applied to MGs requires two stages. The first, known as UC, aims to schedule the on/off switching of the controllable generators and the load/discharge mode of the EESSs to cope with the energy deficit or surplus. The second, known as economic dispatch (ED), aims to minimize the operating cost in MG energy dispatch by defining the hourly energy to be generated by each controllable generation unit turned on, and that stored or delivered by the battery system and supplied by the main grid (Wang et al., 2020). From a mathematical point of view, it is presented as a mixed-integer nonlinear optimization problem (MINLP) (Alvarado-Barrios et al., 2020a; Reddy et al., 2019), due to the binary nature of the off/on decision of controllable generating units and the nonlinearity of the fuel cost curves associated with these units and the grid equations where appropriate. The intermittency of RES production due to weather conditions and demand variability introduces uncertainties into the UC problem. Given these characteristics, stochastic approaches are crucial to address optimal MG management Marneris et al. (2017), Alasali et al. (2019), Stochastic Unit Commitment (SUC), which has motivated several studies in the literature (Khan et al., 2016; Li and Xu, 2014). These approaches contribute to the robustness of the solutions, making them more suitable for real implementation in MGs.

The deterministic formulation has only one forecast scenario, against which the margins for the corrections are applied in real time. This is achieved by imposing that the available committed generation capacity is sufficient to compensate for deviations of net demand from forecasts. The authors in Ghasemi-Marzbali et al. (2021) propose an economic model for the design of an isolated hybrid MG in the Ardabil region of Iran, consisting of a PV, DE, WT and a BESS. It formulates an optimization problem with the objective of minimizing the operating costs of 20 years of operation. To solve it, it uses an Extended Artificial Bee Colony Algorithm (EABC) based on chaos theory. The results obtained show that the proposed model is approximately 2.2% less expensive than other methods. In Kiptoo et al. (2020) a deterministic energy management model for hybrid MG based on RES is presented that considers DR and operates in isolation. The optimization problem is formulated as an MILP problem. The objective is to minimize the total operating costs of the MG, which includes investment costs, maintenance, and demand management. In Rana et al. (2021), a master–slave optimization problem is developed for the hybrid PV-BESS MG connected to the grid. That algorithm incorporates a real-time management subproblem that detects a possible island mode and operates the isolated MG accordingly. The proposed algorithm can control battery charge–discharge operations and ensure optimal use of the PV unit for peak shaving, thus ensuring that the ED minimizes total operating costs.

In Gabriel et al. (2022), optimal penetration rates are proposed for each technology (PV, WT, DE, BESS and DR) that allow minimizing the total operating cost and the cost of unsupplied energy at different horizons of a predominantly residential MG

powered by renewable resources. That work uses an integer linear programming (ILP) approach, utilizing two optimization algorithms based on heuristic approaches, GA and PSO, to achieve demand side management control. The authors in Nemati et al. (2015), Askarzadeh (2018) adopt this approach for the optimal management of a hybrid MG off-grid, evaluating performance improvement over non-predictive heuristic management strategies as a function of forecast uncertainty.

Stochastic programming takes into account the random variables present in the optimization problem, each associated with a probability of occurrence. Several authors have used this technique to analyze optimal energy management in MGs connected to the power grid. In Moretti et al. (2020) they present a robust adjustable formulation, in which they propose an objective function to minimize the expected total operating cost of multi-energy systems and MGs, comprising the cost of fuel and the value of exchanges with external power grids. They adopt a formulation called Affinely Adjustable Robust Optimization (AARO) and, among the possible approaches to handle uncertainty, select the decision rule-based approach, which allows different response strategies, depending on the sign of the forecast error.

In Querini et al. (2021) they present a two-level SUC that integrates the power procurement contract, the uncertainty-driven operating schedule and the response to the demand for connected MGs. They use LINGO optimization software that includes solvers that perform linearization automatically. Economic feasibility studies are applied to the design of a hybrid MG for Gato Colorado, Santa Fe region, Argentina. In Bolurian et al. (2022) three objective functions are considered to optimize operating costs, pollution emission, and flattening of the electricity demand profile of a grid-connected MG. The architecture is made up of nonrenewable generators (DE), RES (WT), and EES and considers a set of adjustable and constant loads. The uncertain behavior of RES production, stochastic modeling of electric loads, and electric power price are modeled using the Monte Carlo technique (MCS). The objective functions have been optimized using the column generation and constraint generation (C&CG) optimization algorithm.

The impact assessment of electric vehicles and the economic feasibility of offloading stored energy from their batteries to the grid (from vehicle to grid) in a MG environment are evaluated in O'Neill et al. (2022). They developed a hybrid residential MG model that includes RES (PV, WT), BESS and DE, using data from Smart Grid Smart City (Australian Government, 2014) and studied four different penetration scenarios. The simulations were performed in openCEM, which is an "open source" power grid modeling tool developed by ITP Analytics (ITP Analytics, 2020). The optimization results include the capacity required and the capacity factors of each generation unit to meet the demand with the lowest operating cost measured by the levelized cost of electricity (LCOE).

The operation of isolated MGs in the presence of DERs becomes very difficult due to the intermittency of the power supply from the RES and the variability of demand. In Alvarado-Barrios et al. (2020a), the design of an EMS for a MG is proposed using the SUC tool in two stages. An optimization problem is presented, whose main objective is to minimize the total operating cost of the MG operating in isolation, consisting of an ED, MT as controllable generation units, WT and PV units as noncontrollable RESs, and a BESS. The problem has been formulated as MILNP in a stochastic environment, by considering the error in the demand prediction, guaranteeing a reliable islanded operation of the MG. It applies an Autoregressive Moving Average Model (ARMA) to predict the demand curve.

Table 1

Relevant literature in optimization of microgrids. Objective Function: Operation Cost (CO), Emission Cost (EC), Compensation Cost of Load Shedding (CCLS), energy contracted/consumed (ECC), power contracted/consumed (PCC), self-healing operation (SHF). Type: Single Objective. Microgrid: Standalone (SA), Grid Connected (GC). Approach: Deterministic Unit Commitment (DUC), Stochastic Unit Commitment (SUC). Strategy: Genetic Algorithm (GA), Enhanced Genetic Algorithm (EGA), ILP, NLP, MILP, MILNP, Binary Particle Swarm Optimization (BPSO).

Ref. no.	Objective function	Type	Microgrid	Uncertainty modeling	Approach/Strategy
Moretti et al. (2020)	min f(OC, EC)	SO	GC	decision-rule-based	SUC (MILP-AARO)
Wang et al. (2020)	min f(OC)	SO	GC	MCS	SUC (ILP)
Alvarado-Barrios et al. (2020a)	min f(OC)	SO	SA	ARMA	SUC (MILP)
Li and Xu (2014)	min f(OC, EC, CCLS, NL)	SO	SA	...	DUC (BPSO)
Ghasemi-Marzbali et al. (2021)	min OC	SO	SA	...	DUC (MILP-EABC)
Kiptoo et al. (2020), Rana et al. (2021)	min OC	SO	SA	...	DUC (MILP)
Gabriel et al. (2022)	min OC	SO	SA	...	DUC (MILP-GA,PSO)
Nemati et al. (2015)	min OC	SO	SA	...	DUC (EGA)
Askarzadeh (2018)	min OC	SO	SA	...	DUC (MGA)
Querini et al. (2021)	min f(OC, ECC, PCC)	SO	GC	chance-constrained	SUC (MINLP)
Bolurian et al. (2022)	min f(OC, EC, CCLS)	SO	GC	MCS	SUC (MILP- C&CG)
O'Neill et al. (2022)	min OC	SO	GC	openCEM	SUC (MILP)
Tostado-Véliz et al. (2022a)	min OC	SO	SA	Stochastic-IGDT	SUC (MILP)
Tostado-Véliz et al. (2022b)	min OC	SO	SA	Forecast Intervals	SUC (MILP)
Thornburg and Krogh (2021)	min OC	SO	SA	PLASMiS (MCS)	SUC (MILP)
Nikkhah et al. (2020)	min OC	SO	SA	Weibull(PDF)	SUC (MINLP-GAMS)
Ahmadi et al. (2020)	min f(OC, SHF)	SO	SA	LHS	SUC (MILP)
Present	min OC	SO	SA	Markov process	SUC(UC-MILP, ED-QP)

In Tostado-Véliz et al. (2022a), an MILP is formulated for optimal scheduling of isolated MGs and DR programs, whose objective is to minimize the impact of possible failures of MG components, thus reducing their detrimental effects on the overall economy and welfare of the autonomous system. To this end, a novel stochastic IGDT model is developed, in which uncertainties in renewable generation and demand are modeled through scenarios (stochastic programming), while failures are modeled using the information gap decision theory (IGDT) method. In Tostado-Véliz et al. (2022b) a new optimal programming model is developed for isolated MGs containing a green hydrogen storage system (HSS) and DR programs. The HSS is modeled using logic rules, and an optimization based on MILP is formulated. Uncertainties in renewable generation and local demand are handled by an original interval formulation and an iterative solution procedure.

The design of PLASMiS, an MCS simulator that evaluates operational strategies for isolated MGs, is presented in Thornburg and Krogh (2021). This software probabilistically models MG operations over time with and without demand side management (DR) for MGs with limited or undersized generation assets. The MG in the case study is located in Rwanda. It is made up of a 12 V lead acid car battery bank, PV, DE, a hydroelectric unit, and WT to supply loads consisting of 40 single-family houses, a hospital, and a factory.

In Nikkhah et al. (2020), an integral coupled framework of UC optimal power flow (OPF) is proposed to investigate the impacts of voltage stability and uncertainty about wind power generation on the power scheduling of isolated MGs in the presence of WT, PV and BESS. The proposed model is a mixed-integer nonlinear programming problem (MINLP), which is solved with existing solvers in GAMS®. To model the WT power output as a stochastic variable, the model uses the Weibull probability density function (PDF) for the uncertainty of the wind speed and the scenario-based approach. A flexible two-level EMS is presented in Ahmadi et al. (2020). The upper-level EMS is responsible for the optimal scheduling of the normal operating MGs, while the lower-level helps the MGs to operate in case of failure in islanded self-heating modes. To account for the uncertainties of the RES-based units and load consumption, he presents a stochastic modeling strategy. Many scenarios of RES-based generation and load consumption are generated using Latin hypercube sampling (LHS) to represent prediction errors over the 24-hour time horizon. Table 1 shows a summary of the literature review.

The literature review shows limitations in the application of optimization techniques to achieve optimal energy management in isolated MGs that can affect their viability, performance and scalability. The following limitations are identified: (i) not adequate treatment of the intermittencies associated with RESs and demand variability, proposing deterministic analyzes in the solution of the UC problem (see Li and Xu (2014), Askarzadeh (2018)), (ii) not considering all sources of uncertainties present (for example, in Alvarado-Barrios et al. (2020a) authors only consider the errors in the demand prediction, neglecting the ones from RESs, in this case, PV and WT), (iii) not taking into account all conditions of wind speed variability and solar irradiance, (e.g. Ghasemi-Marzbali et al. (2021)), (iv) the computational complexity can increase exponentially depending on the uncertainty analysis techniques that are incorporated into the optimization algorithms (e.g. using scenarios, as in the case of MCS (Wang et al., 2020; Bolurian et al., 2022)). The present work contributes to responding to and overcome some of the limitations mentioned above.

Regarding the modeling of uncertainties, in the recent literature, there are different probabilistic methods that consider and model them, mainly caused by RESs to schedule activities in MGs. In Atwa et al. (2009) the authors calculate a probabilistic generation-load model to obtain all combinations of all possible generations of renewable sources. These sources are modeled by probability density functions that are divided into a number of states, each of them having a different probability. In the field of storage scheduling and optimal generation, the authors in Gast et al. (2014) use the persistence wind prediction model to forecast wind power at any time in the future considering only the average wind power of the previous hour. The same method is used in Bejan et al. (2012) where the marginal distributions of errors obtained from the difference between the prediction of the wind power at time $t + h$ and the wind power at time t are approximated by the Laplace distribution.

In this work, in contrast to what was done in Atwa et al. (2009), the probabilities are obtained directly from the application of a homogeneous Markov chain for PV and a nonhomogeneous Markov chain for wind power. The approach aims to incorporate the autocorrelation that exists in these phenomena and to consider the dependence of the power produced in an hour within a day. In particular, wind power shows a different transition probability matrix for each hour of the day, and therefore the chain is not homogeneous. PV power is studied

on the basis of seasonal trend and modeling the residual with the homogeneous Markov chain. This methodology improves the persistence approach done in Gast et al. (2014) because in the non-homogeneous Markov model, the power prediction value depends on the power value at the current time through specific transition probability matrices that change every hour. The suitability of this choice is supported by previous work showing the accuracy of Markov models and some of their extensions in wind speed and power forecasting (Papaefthymiou and Klockl, 2008; Yang et al., 2015; D'Amico et al., 2013, 2014), as well as PVs (Eniola et al., 2019; Li et al., 2008). It is worth noticing that our approach is completely nonparametric and does not need any specification of the model parameters and probability distribution functions, with the exception of the state space of the Markov process. The suitability of this strategy is confirmed by real data.

1.3. Contributions

In this work, the main novelty consists in combining the application of non-homogeneous and homogeneous Markov processes to model the uncertainties of WT and PV in a SUC and ED problem. We join the application of these stochastic models to the MG scheduling problem management, adding stochasticity and uncertainty. In particular, we use 10-year hourly wind speed and solar irradiation data to obtain the Markov probability transition matrices and, consequently, to simulate 100 days of WT and PV powers. Furthermore, demand is modeled using the autoregressive moving average (ARMA) technique to obtain its prediction.

The optimization problem aims to cover demand while minimizing the total cost and is divided into three stages, as in Alvarado-Barrios et al. (2020b). In the first stage, uncertainties are modeled, in the second stage UC and ED are obtained, and in the third stage, a second ED is solved considering a spinning reserve in dispatchable units (DE and MT) to cover the difference between the predicted and actual value of demand.

Furthermore, we consider two different scenarios in which we modify the capacity and maximum power of the BESS to see how these parameters impact the problem.

To get further confirmation, we also compare the results obtained from the proposed strategy in which uncertainties are associated with demand and RES, with the study in Alvarado-Barrios et al. (2020b) in which only the uncertainty associated with demand is considered. We show how RES production affects MG management and total cost.

1.4. Paper organization

The rest of the document is structured as follows. Section 2 shows the structure of the MG and the description of the problem. Section 3 shows the demand models and the sources of electrical energy. In Section 4 the optimization problem and the control strategy are presented. Section 5 shows and explains the results obtained for the different scenarios considered. Finally, the conclusions are presented in Section 6.

2. Proposed energy management system

This section shows the structure of the MG and presents the formulation of the problem, highlighting all the variables that play a fundamental role in it.
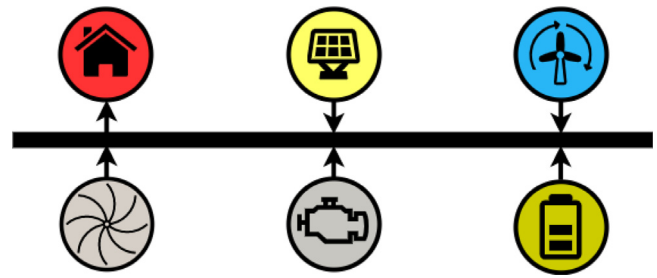

Fig. 1. Microgrid structure.

2.1. Microgrid structure

In this work, an AC MG has been considered, as shown in Fig. 1. It is integrated by a set of interconnected loads and DERs with clearly defined electrical limits such as: DE and a MT as dispatchable units, and a WT and a PV plant as non-controllable RESs. Finally, a BESS integrated by lithium-ion technology batteries acting as a controllable and independent unit is considered. The MG operates disconnected from the main medium and/or low-voltage grid, i.e., in isolation.

2.2. Problem description

When a MG operates in a stand-alone mode, it is necessary to control the distributed energy sources to ensure the voltage and frequency stability of the MG, but in this work a physical network is not considered, so the authors only solve the generation dispatch. Frequency stability is guaranteed because the power balance must be met in order to obtain generation dispatch. The MG concept is vital to manage the growing energy demand through local energy production and to reduce greenhouse gas emissions. Given the presence of intermittent RESs and the variability of demand, stochastic approaches are crucial to address optimal management of MG.

This article proposes the design of the energy system management for a MG using the Stochastic Unit Commitment, considering the uncertainty in demand prediction and the stochastic nature of the wind and solar irradiance.

The power generated by the RESs (PV and WT) is treated as stochastic variables modeled by Markov processes. The powers generated by the dispatchable units (DE and MT), as well as the management of the BESS, are variables of the problem. The hourly scheduling problem of the generation units makes it possible to obtain which dispatchable unit should be connected to the MG and the power to be delivered at each moment.

Management of the energy system proposes an optimization problem whose main objective is to minimize the total operating cost of the MG in a stochastic environment. Fig. 2 shows the procedure proposed in this work for the design of an energy management system for the MG.

The problem is divided into the following three stages:

- In the first stage, given a time series of historical data on demand, wind speed, and solar irradiation, an ARMA model is applied to predict the demand curve together with the calculation of the error in the demand forecast, and the Markov model is applied to simulate wind and PV power. The time horizon is 24 h.
- In the second stage, the SUC is calculated and, consequently, the demand coverage is determined. It is assumed that the spinning reserve provided by conventional generation units (MT and DE) and the BESS is able to cover the error in the
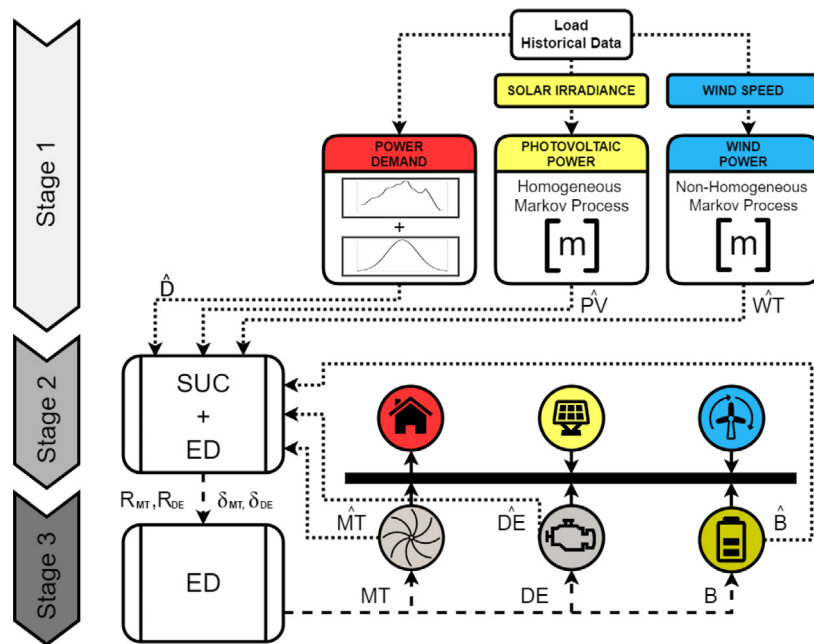
Fig. 2. Flowchart of the problem.

demand forecast. The above condition guarantees the reliable operation of the MG on the island. Therefore, reliability criteria are incorporated into the optimization problem to ensure this.

- In the third stage, the real-time operation of the MG is modeled and it is observed that there is a difference between the demand prediction and the actual value, giving rise to a new spinning reserve value. Then, a second optimization problem is solved, in which it is decided which generators have to cope with the demand variation, so that the operating costs are minimized.

3. System modeling

3.1. Demand

The demand for power is predicted for the next 24 h, using an ARMA model, applied on 2-year historical data from Sardinia (Italy), as it was done in Alvarado-Barrios et al. (2020b), Pappas et al. (2008). The equation describing the demand model is as follows:

$$D(t) = \sum_{i=1}^{p} \phi_i D(t-i) + \sum_{j=0}^{q} \theta_j \varepsilon(t-j), \tag{1}$$

where $D(t)$ is the demand at current time t, θ_j and ϕ_i are the coefficients of the moving averages and the autoregressive model, respectively, and $\varepsilon(t-j)$ are errors due to predictions. The model makes demand depend on its antecedent p values and on the antecedent q values of the errors. The latter two parameters are calculated by using the Akaike's Information Criterion. $\varepsilon(t-j)$ are calculated as relative forecast error percentages in each hour and fit a normal distribution. The 3σ criterion is applied, which gives a range where the demand error will be for $99,73\%$ of the cases. In the scenarios studied, demand $D(t)$ consists of its forecast $\hat{D}(t)$ plus an actual value of the error within the range $\omega(t)$, as shown in Section 4.3.

3.2. Wind generation

We consider 10 years of hourly wind speed data, precisely from 01/08/2008 to 01/08/2018, which refer to a location in Sardinia with geographical coordinates of 39,5N latitude and 8,75E longitude (G.E.S. Data, I.S.C.G. DISC, 2015a). To obtain the production of wind power from the wind speed data, the WT power curve is taken in the analytical form shown in Eq. (2) (Tapia et al., 2003; Lei et al., 2006).

$$WT(t) = \begin{cases} 0 & \text{for} & v < v_{ci}, \\ P_r \frac{v^3 - v_{ci}^3}{v_r^3 - v_{ci}^3} & \text{for} & v_{ci} < v < v_r, \\ P_r & \text{for} & v_r < v < v_{co}, \\ 0 & \text{for} & v > v_{co}, \end{cases} \quad \forall t \in \{1, 2, \dots, 24\} \tag{2}$$

P_r and v_r represent the rated power (kW) and the wind speed (m/s), respectively, and v_{ci}, v_{co} and v are the cut-in, cut-out and actual wind speed, respectively. The power curve is shown in Fig. 3. In particular, the WT produces power for a wind speed higher than or equal to 4 m/s, and production becomes constant for a wind speed greater than or equal to 13 m/s.

Data are scaled to have a maximum wind power output on the grid equal to 80 kW to have the same maximum wind energy supply as we find in Alvarado-Barrios et al. (2020b). Wind energy production is modeled as a non-homogeneous Markov reward process (D'amico et al., 2018). A random variable J_n^{WT} is considered with values in the set $E^{WT} = \{1, 2, 3, 4, 5\}$ that denote the different levels of wind power generated by the system. In the following, a precise identification of the values of the elements of E^{WT} will be given later. J_n^{WT} indicates the state of the system at the transition nth. Each transition from one hour to the next is governed by a probability transition matrix that depends on the time of day the system is in. Analyzing the actual data yields 23 probability transition matrices that satisfy the following relationship:

$$P[J_{n+1}^{WT} = j \mid J_n^{WT} = i_n, J_{n-1}^{WT} = i_{n-1}, \dots, J_1^{WT} = i_1,$$
$$J_0^{WT} = i_0] = P[J_{n+1}^{WT} = j \mid J_n^{WT} = i_n] = p_{i_n j}(n+1). \tag{3}$$

Fig. 3. The power curve.

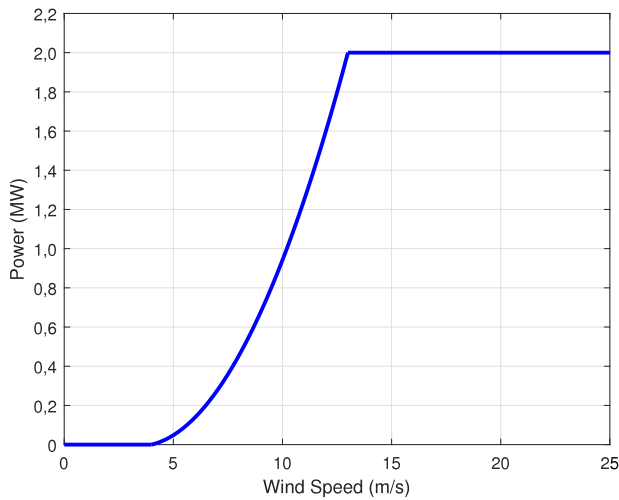**Fig. 4.** Hourly average of the wind power production in a day for real and simulated data.

In practice, the transition matrices change over time. Defining $\phi(s, t) = (\phi_{ij}(s, t))_{i,j \in E^{WT}}$, $s, t \in \mathbb{N}$, as a matrix function with the elements obtained by $\phi_{ij}(s, t) = P[J_t = j \mid J_s = i]$, that is, $\phi_{ij}(s, t)$ denotes the probability of having a wind power equal to j at time t, given that at time s the wind power generated was equal to i. Therefore, the transition probability function can be obtained according to the following equation:

$$\prod_{k=s+1}^{t} P(k) = \phi(s, t), \quad s, t \in \mathbb{N}, \quad 0 \le s \le t. \tag{4}$$

The states of the set E are five because the power output is divided into five ranges according to its value. Specifically, state 1 corresponds to the power values between 0 and 16 kW, state 2 corresponds to the power values between 16 and 32 kW, state 3 corresponds to the power values between 32 and 48 kW, state 4 corresponds to the power values between 48 and 64 kW, and state 5 corresponds to power values between 64 and 80 kW. Once the states of the non-homogeneous Markov chain are represented, a random reward is assigned to each state with the intention of assigning to each state a specific wind power production belonging to the intervals that identify the states of E^{WT}. This is done by extracting a random value from the set of wind power data classified in the corresponding state. In this way, the simulation of 10-year wind power production data is obtained. Fig. 4 shows a comparison between the hourly average of the real and simulated wind power productions obtained by the non-homogeneous Markov reward process. It is evident that the two curves follow the same trend over time and this demonstrates the validity of the Markov reward process approach.

As an example, two probability transition matrices are shown: matrix (5) referring to hours $2:00 - 3:00$ a.m. and matrix (6) referring to hours $8:00 - 9:00$ a.m.

$$\begin{array}{c} \\ 1 \\ 2 \\ 3 \\ 4 \\ 5 \end{array} \begin{array}{ccccc} 1 & 2 & 3 & 4 & 5 \\ \begin{pmatrix} 0.98 & 0.02 & 0 & 0 & 0 \\ 0.10 & 0.80 & 0.10 & 0 & 0 \\ 0 & 0.16 & 0.73 & 0.10 & 0.01 \\ 0 & 0 & 0.27 & 0.64 & 0.09 \\ 0 & 0 & 0.01 & 0.10 & 0.89 \end{pmatrix} \end{array} \tag{5}$$
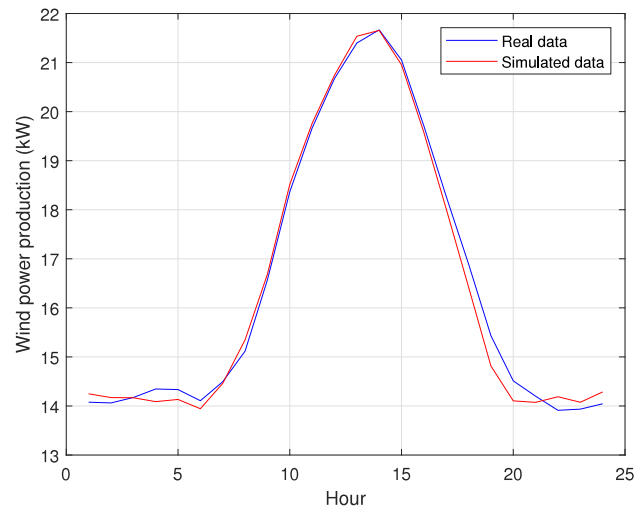
$$\begin{array}{c} \\ 1 \\ 2 \\ 3 \\ 4 \\ 5 \end{array} \begin{array}{ccccc} 1 & 2 & 3 & 4 & 5 \\ \begin{pmatrix} 0.94 & 0.05 & 0.01 & 0 & 0 \\ 0.15 & 0.63 & 0.20 & 0.02 & 0 \\ 0.01 & 0.13 & 0.57 & 0.24 & 0.05 \\ 0 & 0 & 0.07 & 0.43 & 0.50 \\ 0 & 0 & 0 & 0.05 & 0.95 \end{pmatrix} \end{array} \tag{6}$$

For example, if it is the hour $2:00$ in the morning and the state of the chain is equal to 1, the probability that the next state is again equal to 1 is 98%. Similarly, if it is $8:00$ a.m. and the state of the chain is equal to 2, the probability that the next state is equal to 2 is 63%.

3.3. Photovoltaic generation

10 years of hourly solar irradiation are taken from 2008/08/01 to 2018/08/01 at the same geographical coordinates considered for the wind speed data (G.E.S. Data, I.S.C.G. DISC, 2015b). Taking into account Eq. (7) to obtain the PV power (Lasnier and Ang, 1990):

$$PV(t) = P_{STC} \frac{n \cdot E_{M,t}}{E_{STC}} [1 + h(T_{M,t} - T_{STC})], \quad \forall t \in \{1, 2, \dots, 24\} \tag{7}$$

where $PV(t)$ is the output power of the PV plant at time t, $E_{M,t}$ and $T_{M,t}$ is the solar irradiance and the module temperature at time t, and P_{STC}, E_{STC} and T_{STC} are the maximum power, the irradiance, and the temperature under Standard Test Conditions (STC), respectively. Finally, n denotes the number of PV panels, h the power temperature coefficient (%/°C). Data are scaled to have a maximum PV power output in the grid equal to 40 kW. Again, the motivation for this choice is to have the same maximum PV source power supply as in the study in Alvarado-Barrios et al. (2020b). PV power is detrended by computing the average hourly power for each month of the year and calculating the difference between this and the PV power data. In this way, residuals are obtained and modeled using a homogeneous Markov reward process (D'Amico et al., 2021). In this case, a random variable J_n^{PV} with values in the set $E^{PV} = \{1, 2, 3\}$ is considered. In this case, the states in the space E^{PV} are three because the residuals are divided according to whether they are positive, negative, or equal to 0. J_n^{PV} indicates the state of the system at the nth transition. Analyzing the actual data yields a probability transition matrix
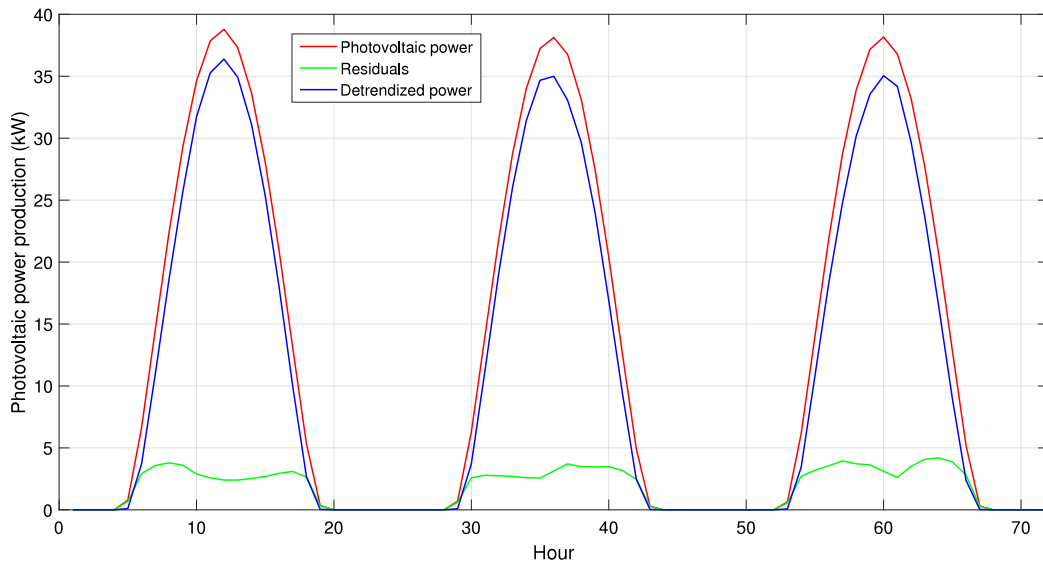
Fig. 5. 72-hour sample of hourly PV power production, detrendized power and residuals.
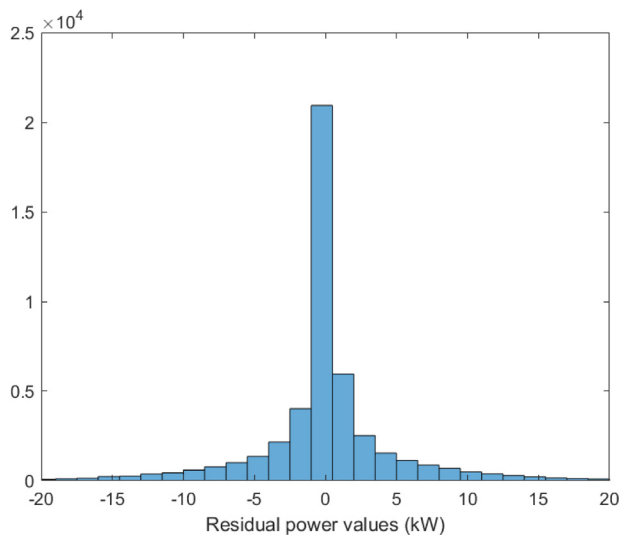

Fig. 6. Histogram of the residual values.

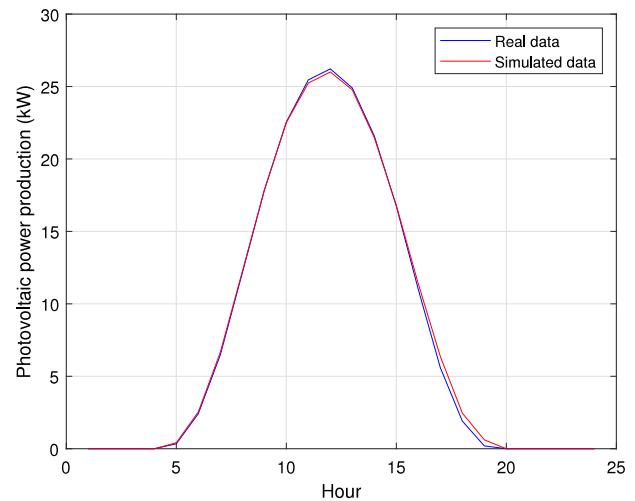**Fig. 7.** Hourly average of the PV power production in a day for real and simulated data.

that satisfies the following relation:

$$P[J_{n+1}^{PV} = j \mid J_n^{PV} = i_n, J_{n-1}^{PV} = i_{n-1}, \ldots, J_1^{PV} = i_1,$$

$$J_0^{PV} = i_0] = P[J_{n+1}^{PV} = j \mid J_n^{PV} = i_n] = p_{ij}. \tag{8}$$

In this case, the transition probabilities of the Markov chain that represents the production of PV energy are independent of time n, so the process is said to be homogeneous over time.

For the probability transition matrix $P = (p_{i,j})_{i,j \in E^{PV}}$, the simulated residual Markov chain is obtained and a reward is substituted for each state of the chain, randomly extracting a value from the set of values that are in the corresponding state.

In practice, the detrended power is obtained, to which we add the simulation of the residuals over time. A 72-hour sample of this methodology is shown in Fig. 5, where it is observed that the PV energy production is higher than the detrended power and this fact produces positive residuals in the central hours of each day. The histogram of the residual values is shown in Fig. 6 and it can be seen that the largest number of values are close to zero.

In Fig. 7 it is evident that the hourly average of the real and simulated PV powers follows the same trend over time.

The probability transition matrix (9) of the residual Markov chain is shown below.

$$\begin{array}{c} \\ 1 \\ 2 \\ 3 \end{array} \begin{array}{ccc} 1 & 2 & 3 \\ \begin{pmatrix} 0.91 & 0.04 & 0.05 \\ 0.08 & 0.82 & 0.10 \\ 0.08 & 0.10 & 0.82 \end{pmatrix} \end{array} \tag{9}$$

For example, if the state of the chain is equal to 2, the probability that the next state is again equal to 2 is 82%.

3.4. Microturbine and diesel engine

The non-renewable sources connected to the MG are the MT and the diesel engine. The power generated by these conventional generators is physically limited within the limits and is modeled with Eqs. (10).

$$DE_{min} \leq DE(t) \leq DE_{max}$$

$$MT_{min} \leq MT(t) \leq MT_{max} \tag{10}$$

$$\forall t \in \{1, 2, \ldots, 24\}$$

DE_{min} and DE_{max} define the minimum and maximum power limits of the DE, and MT_{min} and MT_{max} are the power limits of the MT generator.

3.5. Spinning reserve

Spinning reserve is the additional generation capacity available by increasing the power output of the generators (Rebours and Kirschen, 2005; Ortega-Vazquez and Kirschen, 2007). In this work, the spinning reserve is composed of a diesel engine $R_{DE}(t)$ and a MT generator $R_{MT}(t)$, and can be expressed at each time through Eqs. (11).

$$R_{DE}(t) = DE_{max} - DE(t)$$
$$R_{MT}(t) = MT_{max} - MT(t) \tag{11}$$
$$\forall t \in \{1, 2, \ldots, 24\}$$

3.6. Energy storage system

The battery is a storage energy element that can work as a generator or as a consumer at each time, so the state of charge (SOC) must be updated at each time through Eqs. (12) (Chen et al., 2011b).

$$SOC(t) = SOC(t-1) - \begin{cases} \Delta t \cdot B(t) \cdot \eta_c & \text{for} \quad B(t) < 0 \\ \frac{\Delta k \cdot B(t)}{\eta_d} & \text{for} \quad B(t) > 0 \end{cases} \tag{12}$$
$$\forall t \in \{1, 2, \ldots, 24\}$$

where η_c, η_d and Δt are, respectively, the efficiency of charging and discharging and the time between samples. If the battery works as a generator, the power value $B(t)$ is positive and negative in the opposite sense. Furthermore, the SOC must not exceed the maximum and minimum limits to avoid damage. Therefore, it must satisfy Eq. (13).

$$SOC_{min} \leq SOC(t) \leq SOC_{max} \tag{13}$$
$$\forall t \in \{1, 2, \ldots, 24\}$$

3.7. Power balance

The power balance means that power generation must be equal to the power consumed at each time k. This is expressed in Eq. (14).

$$DE(t) + MT(t) + PV(t) + WT(t) + B(t) = D(t) \tag{14}$$
$$\forall t \in \{1, 2, \ldots, 24\}$$

where $DE(t)$, $MT(t)$, $PV(t)$, $WT(t)$, $B(t)$ and $D(t)$ are, respectively, diesel engine, MT, PV, WT and battery power and power demand at time t.

4. Optimization and control strategy

For optimization processes, the predicted values of variables v are taken, which will be noted by $\hat{v}$.

4.1. Unit commitment and economic dispatch

For the proposed strategy to operate the MG, a two-step optimization program is followed, similar to the real way in which electricity grids are managed. The forecast of demand and noncontrollable sources, denoted as $d(t)$:

$$\hat{d}(t) = [\hat{D}(t), \hat{P}(t), \hat{W}(t)], \tag{15}$$

where $\hat{D}(t)$ is the forecast of demand and $\hat{P}(t)$ and $\hat{W}(t)$ are the forecasts of solar and wind powers, respectively.

Table 2
Parameters of each device of the microgrid (Alvarado-Barrios et al., 2020b).

Source	P_{max} (kW)	P_{min} (kW)
MT	20	5
DE	150	15
WT	80	0
PV	40	0

Operational controllable sources are denoted by $u(t)$:

$$u(t) = [\delta_{MT}(t), \delta_{DE}(t), B(t), MT(t), DE(t)]. \tag{16}$$

The decision on how much operational controllable sources should contribute is calculated, as above, in two separate steps. The first step is known as UC. It only decides whether a plant is on or off. For this purpose, binary variables $\delta_{MT}(t)$ and $\delta_{DE}(t)$ are used. Sometimes, it also provides an estimate of the power they will have to supply the next day. The UC has a decision horizon of one day. ED is the name of the second step in which, due to the error between the forecasts and the actual needs, the actual power to be supplied by the controllable sources is decided. This process uses the measured values of the noncontrollable signals so far, and can also use future forecasts to calculate its decision. The state of the plant is the SOC of the battery.

4.2. Objective and constraints

UC and DE will depend on minimizing operating costs. Production values must be chosen that satisfy demand with the minimum associated cost. Thus, together with the production constraints (see Table 2), the energy production must satisfy the following constraint for all time steps t:

$$D(k) = PV(t) + WT(t) + B(t) + \delta_{MT}(t) \cdot MT(t) + \delta_{DE}(t) \cdot DE(t). \tag{17}$$

At an operating point, the DE and the MT will have power available due to inertia, called the spinning reserve. We can define it as the difference between the maximum power the generator can deliver, and the power that is generating at a given instant t:

$$R_{DE}^u(t) = DE_{max} - DE(t)$$
$$R_{MT}^u(t) = MT_{max} - MT(t) \tag{18}$$

These powers have an associated cost, which depends on them and must also be minimized. From the prediction model developed in Section 3.1, a load prediction is obtained for each time step t, $\hat{D}(t)$, with an error with normal distribution $\mathcal{N}(\mu_t, \sigma_t^2)$. Regarding the ARMA model described in Section 3.1, it can be seen that in 99.73% of the cases, the prediction error will be within the interval $[\mu_t - 3\sigma_t, \mu_t + 3\sigma_t]$. Thus, the total spinning reserve must be at least greater than three times the statistical deviation, to satisfy, with the described uncertainty, the power demanded.

$$R_{DE}^u(t) + R_{MT}^u(t) \geq 3\sigma_t \tag{19}$$

Moreover, as a further constraint, the difference in power between the generated power at time t and the minimum power must be greater than or equal to $3\sigma_t$, that is,

$$R_{DE}^d(t) = DE(t) - DE_{min}$$
$$R_{MT}^d(t) = MT(t) - MT_{min} \tag{20}$$

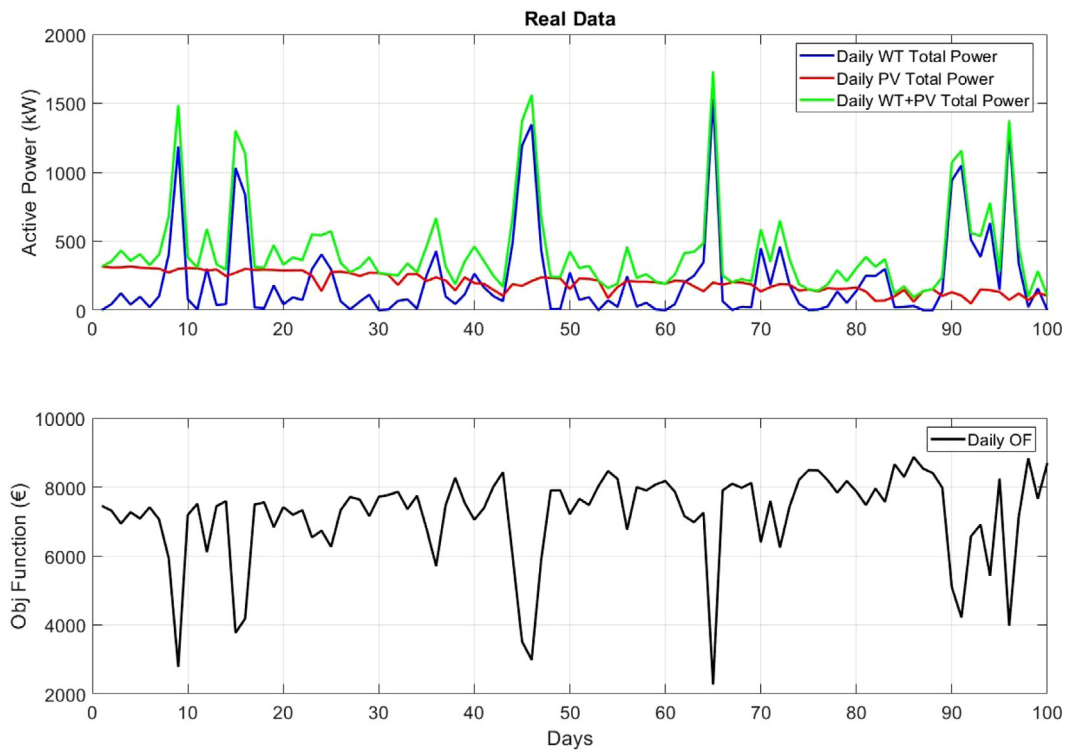$$R_{DE}^d(t) + R_{MT}^d(t) \geq 3\sigma_t \tag{21}$$

Fig. 8. Daily WT, PV and Total Power Sum of 100-day real data sample and the corresponding value of the daily objective function.
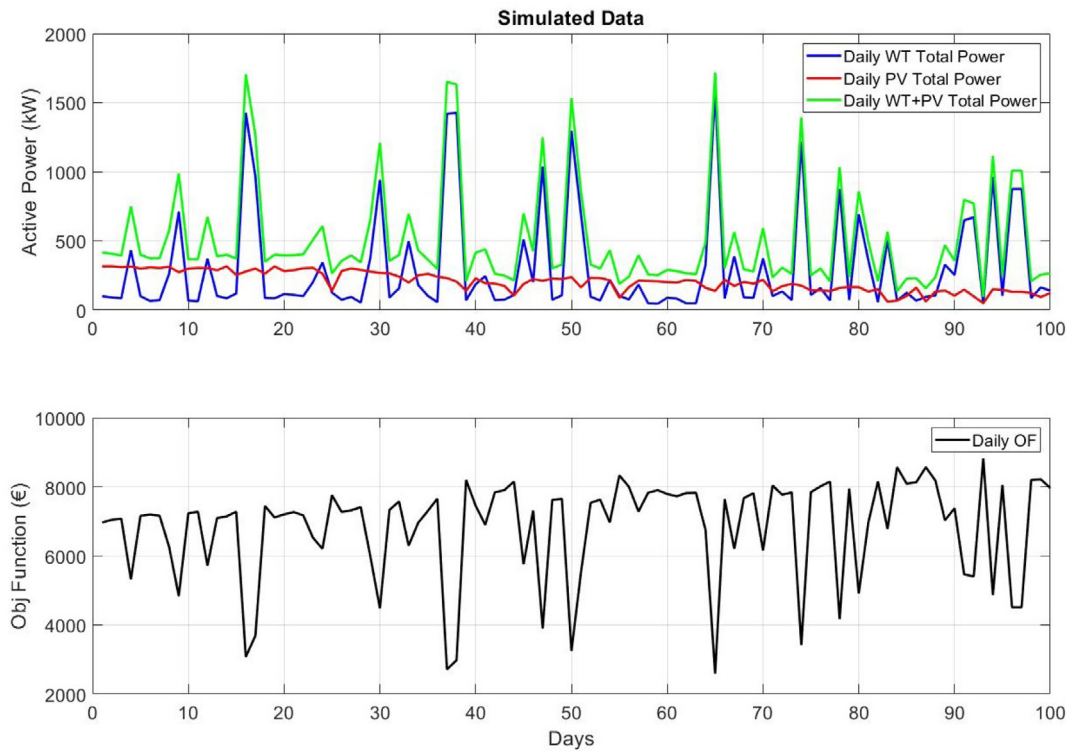

Fig. 9. Daily WT, PV and Total Power Sum of 100-day simulated sample and the corresponding value of the daily objective function.

Control actions that minimize costs on a prediction horizon N are calculated; that is, if horizon N is 24, there are 72 decision variables.

4.3. Optimization algorithm

If C_{MT} and C_{DE} are the costs associated with MT and DE, respectively, for each time step t and for $j = 0 \ldots, N - 1$, the
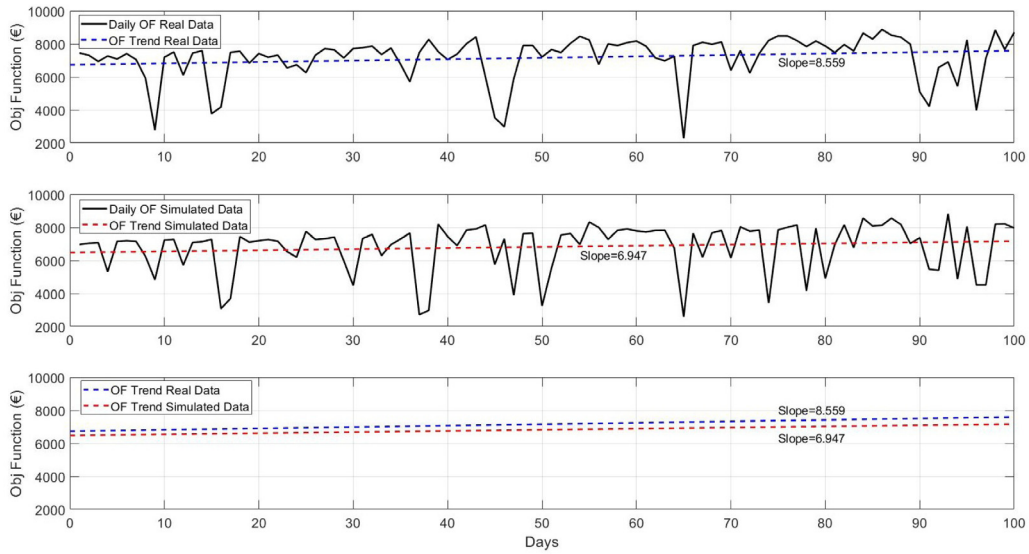
Fig. 10. Daily objective functions of 100-day real and simulated data and the corresponding linear interpolation and slopes for Scenario 1.
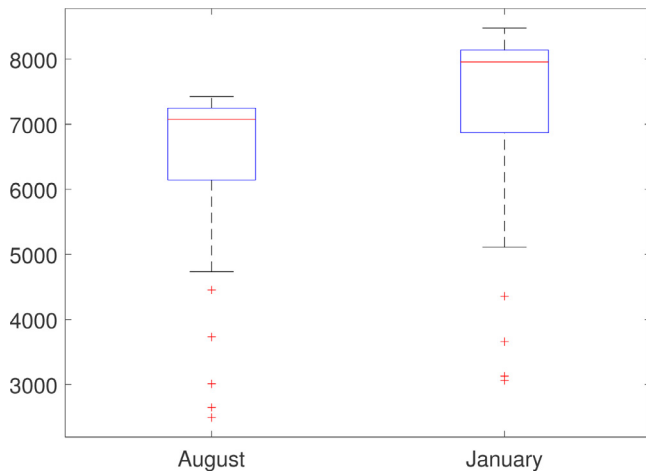
Fig. 11. 50 simulations of the objective function referred to the days 10th January 2019 and 10th August 2019 and the corresponding average.

optimization problem can be formulated as:

$$\min_{\substack{\delta_{MT}, \delta_{DE}, \\ B, MT, DE}} \sum_{j=0}^{N-1} \left(C_{MT}(\delta_{MT}(j), M(j)) + C_{DE}(\delta_{DE}(j), DE(j)) \right.$$

$$\left. + C_{R_{DE}} R^u_{DE}(j) + C_{R_{MT}} R^u_{MT}(j) \right) \tag{22a}$$

$$\text{s.t. } \hat{D}(t+j) = \hat{P}V(t+j) + \hat{W}T(t+j)$$

$$+ B(j) + MT(j) + DE(j) \tag{22b}$$

$$S\hat{O}C(j+1|t) = f\left(S\hat{O}C(j|k), B(j)\right) \tag{22c}$$

$$S\hat{O}C(0) = SOC(t) \tag{22d}$$

$$S\hat{O}C(j|t) \in \mathcal{S}, \tag{22e}$$

$$\delta_M T(j), \delta_{DE}(j) \in \{0, 1\} \tag{22f}$$

$$MT(j), DE(j), B(j) \in \mathcal{E} \tag{22g}$$

$$R^u(j) \geq 3\sigma_j \tag{22h}$$

$$R^d(j) \geq 3\sigma_j \tag{22i}$$

Where $\hat{D}(t+j)$, $\hat{P}V(t+j)$ and $\hat{W}T(t+j)$ are the predicted demand, PV and WT power, respectively, at time t, for the next

steps j. $S\hat{O}C(j+1|t)$ is the prediction of the SOC for the time $j+1$, at the current instant t, which starts with its current value $SOC(t)$ and its dynamic evolution will depend on the previous SOC and the battery power (22d). The sets $\mathcal{S}$ and $\mathcal{E}$ are the battery charge and power limits, respectively.

In the second optimization problem (ED), it is assumed that the binary variables $\delta_{MT}(t)$, $\delta_{DE}(t)$ remain constant and the actual demand, which differs from the expected demand, is known.

$$D(t) = \hat{D}(t) + \omega(t) \tag{23}$$

And the decision variables will be the power increments that optimize the cost, taking into account the actual demand. In this case, the objective function is as follows:

$$\min_{\Delta MT, \Delta DE, \Delta B} \sum_{j=0}^{N-1} \left[a_{MT}\delta_{MT}(j) + b_{MT}(MT(j) + \Delta MT(j)) \right.$$

$$+ c_{MT}(MT(j) + \Delta MT(j))^2 \tag{24a}$$

$$+ a_{DE}\delta_{DE}(j) + b_{DE}(DE(j) + \Delta DE(j))$$

$$\left. + c_{DE}(DE(j) + \Delta DE(j))^2 \right]$$

$$\text{s.t. } \omega(j) = \Delta MT(j) + \Delta DE(j) + \Delta B(j), \tag{24b}$$

$$DE_{min}\delta_{DE}(j) \leq DE(j) + \Delta DE(j) \leq DE_{max}\delta_{DE}(j),$$

$$MT_{min}\delta_{MT}(j) \leq MT(j) + \Delta MT(j) \leq MT_{max}\delta_{MT}(j),$$

$$S\hat{O}C(j+1|t) = f\left(S\hat{O}C(j|t), B(j) + \Delta B(j)\right),$$

$$S\hat{O}C(0) = SOC(t),$$

$$S\hat{O}C(j|t) \in \mathcal{S},$$

$$MT(j) + \Delta MT(j), DE(j) + \Delta DE(j), B(j) + \Delta B(j) \in \mathcal{E}$$

5. Results

This section shows the parameter values for any scenario and presents the results.

5.1. Microgrid data

The parameters of the microgrid devices are listed in Table 2. Regarding the BESS, two different scenarios are considered in which the maximum power and capacity are modified. In the scenarios 1 and 2, the same system characteristics used
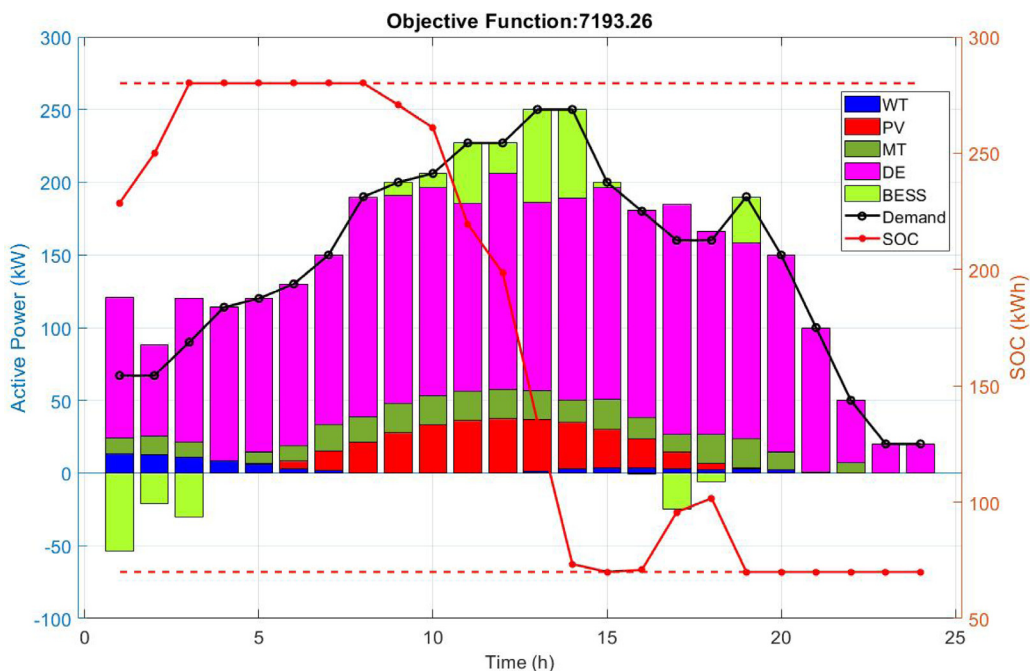
Fig. 12. Demand coverage curve of the day 10th August in real data for Scenario 1.
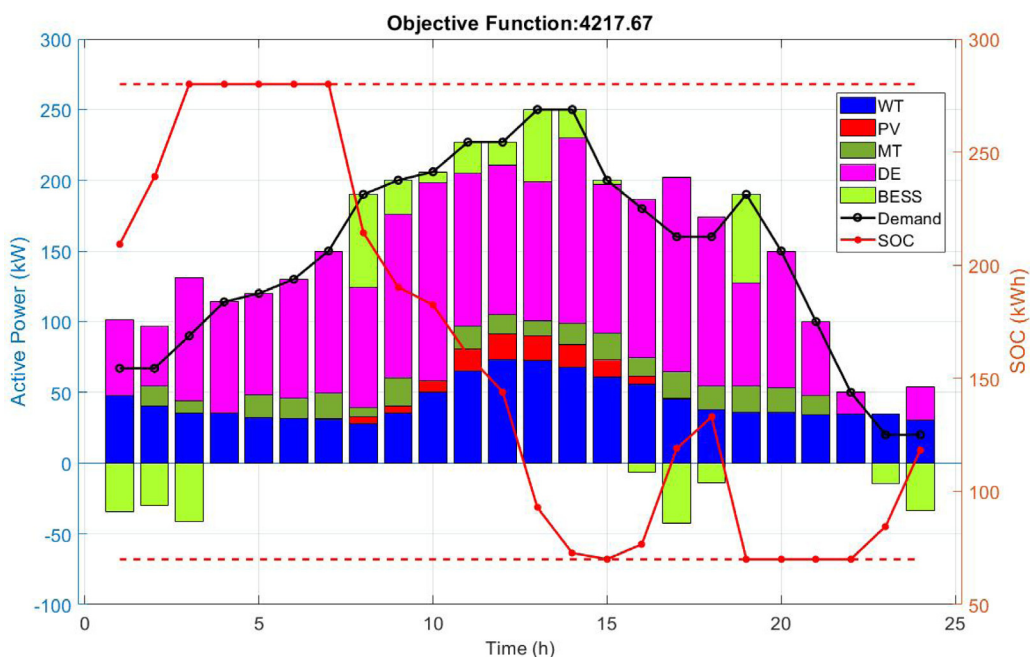

Fig. 13. Demand coverage curve of the day 30th October in real data for Scenario 1.

in Alvarado-Barrios et al. (2020b) are considered for the scenarios the authors called "case 2" and "case 4", respectively. The parameters of the BESS used in each scenario are shown in Section 5.2.

5.2. Simulation results

In this subsection, the results of the scheduling problem are shown, highlighting the importance of considering the uncertainty of RESs in the optimization process. As specified above, two scenarios are calculated in which only the characteristics of the BESS are changed, as can be seen in Table 3.

Table 3
Parameters of the BESS in the different scenarios (Alvarado-Barrios et al., 2020b).

Source	P^c_{max} (kW)	P^d_{max} (kW)	SOC_{min} (kWh)	SOC_{max} (kWh)
Scenario 1	80	80	70	280
Scenario 2	120	120	0	280

As seen subsequently, the value of the objective function is strictly influenced by the contribution of WT and PV power for both scenarios studied.

Regarding the computational cost, daily simulations (hourly time step) are carried out on an Intel(R) Core(TM) i7-8750H CPU
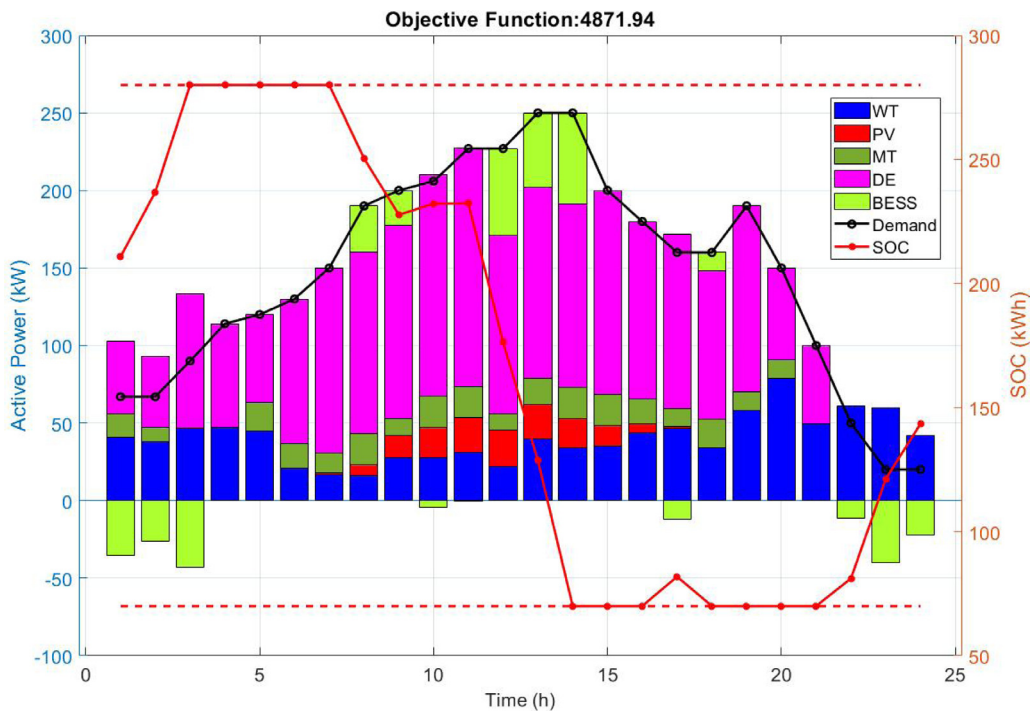
Fig. 14. Demand coverage curve of the day 2nd November in simulated data for Scenario 1.

2.21 GHz laptop and the average CPU time for each simulation is 2.51 min. To perform the 100-day simulations, the CPU time is equal to approximately 4.18 h.

5.2.1. Scenario 1

First, Scenario 1 is considered, in which the power and capacity of the BESS are lower than in Scenario 2. The optimization results for the real and simulated data in the 100-day sample, respectively, are shown in Figs. 8 and 9.

In both cases, it can be seen that an increase in wind power production leads to a decrease in the objective function, and it is clear that wind power is the renewable source that most influences the total cost value. The trend of PV power decreases over time because the first 100 days of our data are considered, this means that the data start on 1 August and end in November. This fact makes the contribution of this renewable source decreasing over time and this influences the trend of the objective function, which obtains a positive slope over time. We can observe this phenomenon for both real and simulated data, and we highlight it in Fig. 10. The total of the objective function and its average calculated from the real data are € 716460 and € 7164.6, respectively. The same results for the simulated data are € 684110 and € 6841.1, respectively. As can be seen, the values obtained are very close. Furthermore, the days 10 January 2019 and 10 August 2019 and d 50 simulations of each are randomly chosen to obtain the objective function. In particular, we keep the detrended PV power of the considered day constant and simulate the residuals for PV power and wind power as shown above. The box plot in Fig. 11 shows that the mean of the objective function is higher and equal to € 7280.9 for 10 January when the contribution of PV power is lower because it is winter. For 10 August 2019, it is equal to € 6054.6. This result shows that the variability of the objective function in one day is considerably high.

In Figs. 12 and 13 we show the demand coverage curves on a day with a small contribution of wind power and on a day in which the contribution of the power produced from the WT is
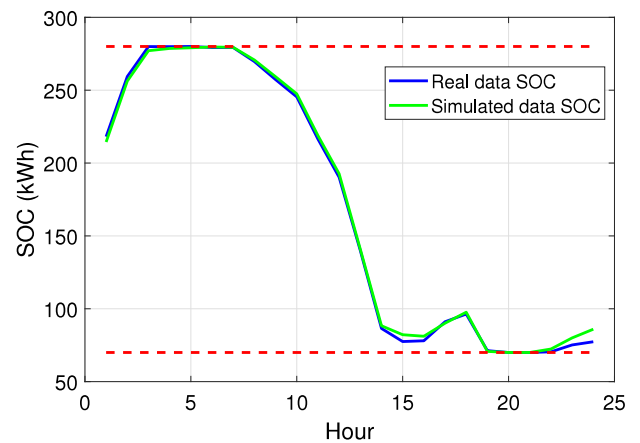

Fig. 15. Hourly SOC mean for 100-day real and simulated data for Scenario 1.

considerably high, respectively. In Fig. 14 the demand coverage curve is shown on a simulated day. In both real and simulated cases, we can see that wind power influences the final value of the objective function and the final SOC of the battery being equal to 0 the day in with the wind contribution is low. In Fig. 15 it is evident that the hourly SOC mean follows the same trend for real data and simulations, reaching maximum values in the first part of the day and presenting values almost equal to the minimum SOC level in the final hours when the contribution of RESs tends to decrease. Figs. 16(a) and 16(b) show the UC result indicating how many times in the real sample of 100 days the MT and the DE are off at each hour of the day. DE is off only the last 3 hours of the day, whereas MT presents a more widespread behavior, but always with a higher probability of being off the last 3 hours. This result is in line with the one obtained in Alvarado-Barrios et al. (2020b). The same behavior is shown for the simulated case in Figs. 17(a) and 17(b).
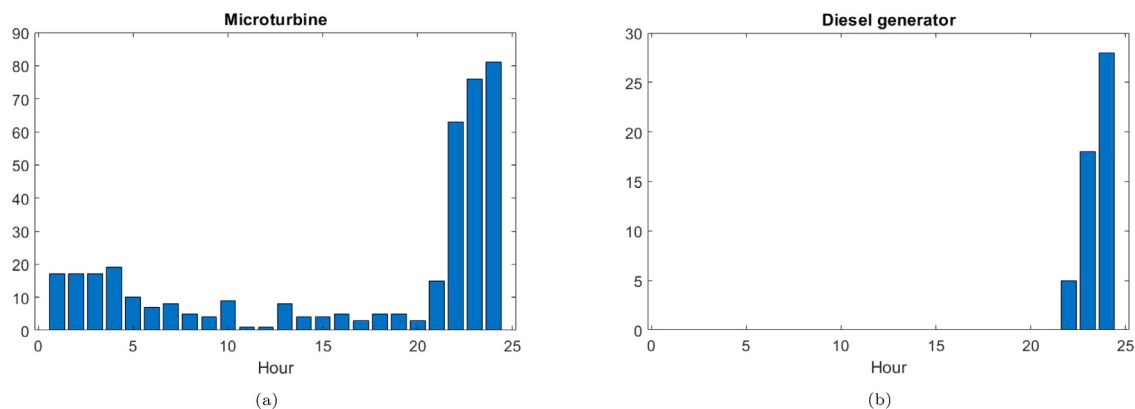
Fig. 16. Hourly off-status histograms of MT (a) and DE (b) for the real 100-day sample for Scenario 1.
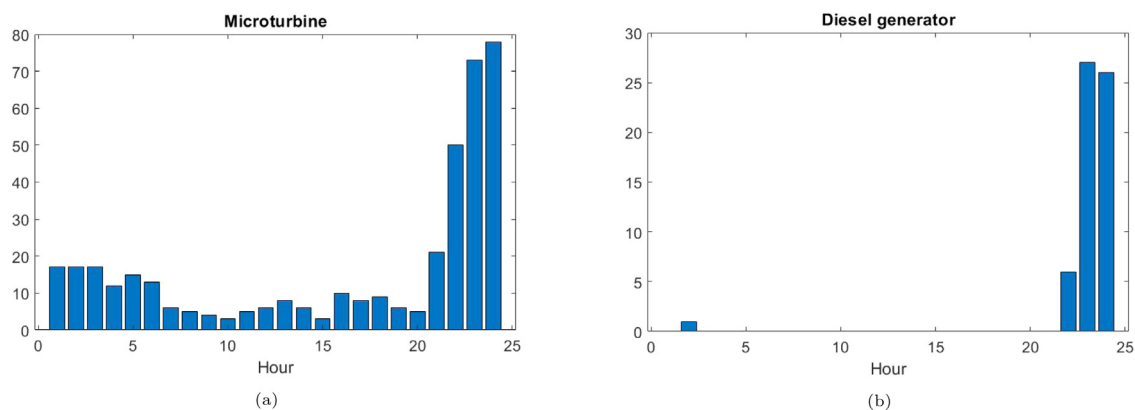

Fig. 17. Hourly off-status histograms of MT (a) and DE (b) for the simulated 100-day sample for Scenario 1.
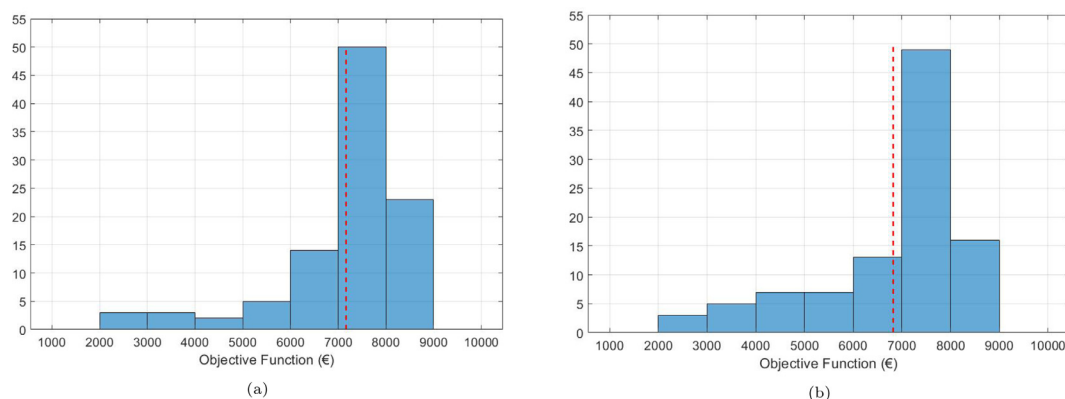

Fig. 18. Objective function histograms of real (a) and simulated data (b) with the indication of the mean value for Scenario 1.

5.2.2. Comparative analysis for Scenario 1

Comparing the mean of the objective function of Scenario 1 (which is equal to € 7164.6) with the result obtained in Alvarado-Barrios et al. (2020b) for the scenario called "case 2", the result of the objective function in €, is equal to € 3159.38 and this means that the authors consider an optimistic scenario in which the contribution of wind energy is high on the day considered. These results can be compared because the optimization has the same boundary conditions and the optimization process used in the paper. This underscores the importance of considering the stochastic nature of RESs. This is also confirmed by looking at the histogram in Fig. 18(a), where most of the values of the objective function are greater than € 7000. Furthermore, a very

similar result is obtained for the simulated data, as can be seen in Fig. 18(b).

5.2.3. Scenario 2

In Scenario 2 the power and capacity of the BESS increase, compared to scenario 1. In this scenario, results are obtained that confirm the results obtained in Scenario 1. Fig. 19 shows the daily objective functions and linear interpolation with information on the slope of the real and simulated 100-day data and the slopes. Also, in this case, the trend of the real and simulated cases is similar with slope values close to each other.

The histogram of the values of the objective functions of the real data sample of 100 days is shown in Fig. 25(a). It is evident that most of the values are greater than € 6000 and the objective
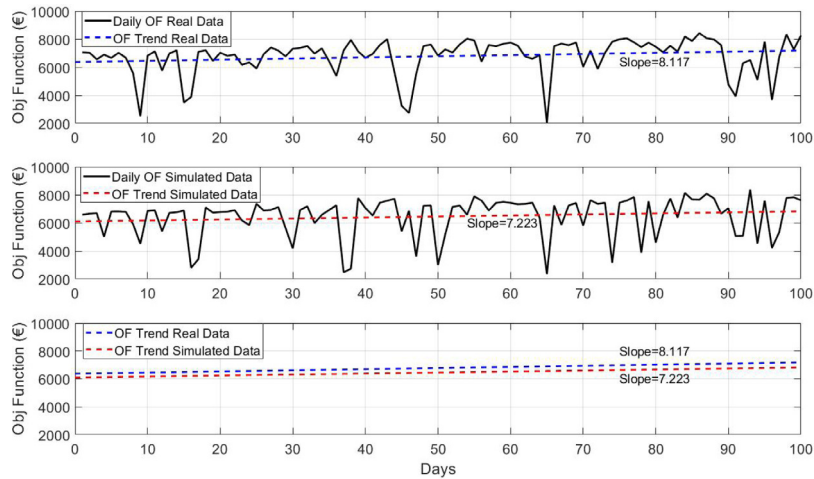
Fig. 19. Daily objective functions of 100-day real and simulated data and the corresponding linear interpolation and slopes for Scenario 2.
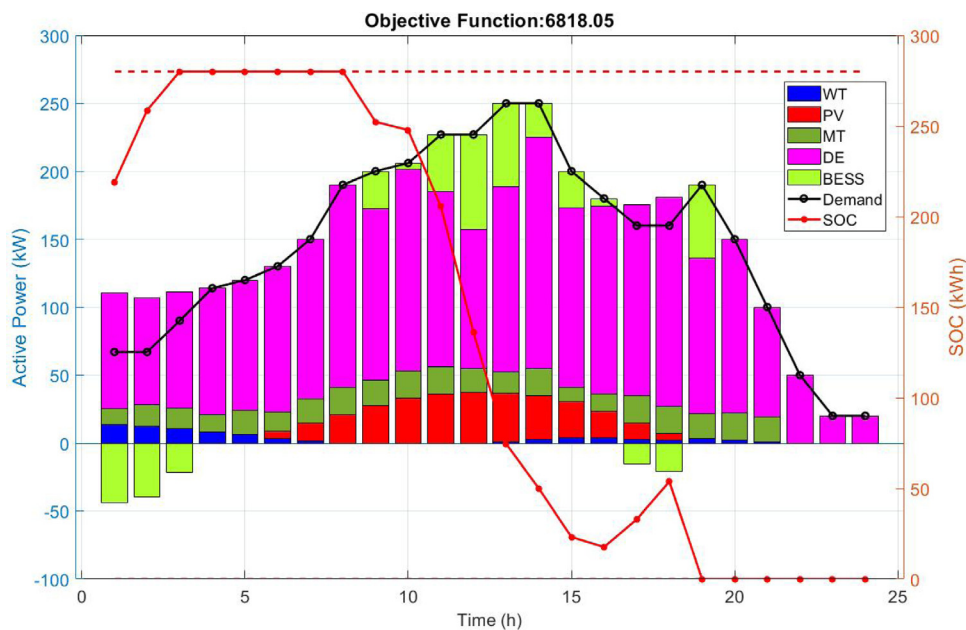

Fig. 20. Demand coverage curve of the day 10th August in real data for Scenario 2.

function average is equal to € 6779.6, which is less than the one obtained in Scenario 1 (€ 7164.6). This is due to the fact that in Scenario 2 we consider a BESS with a higher P_{max} in both charge and discharge and a lower minimum SOC limit, which corresponds to a larger capacity. Figs. 20–22 show the demand coverage curves for the real and simulated data and for the same days considered in Scenario 1. These figures have many similarities with those obtained in the first scenario, and even in this scenario, it can be seen that the SOC level at the end of the day is highly influenced by the existence or absence of wind during the day.

Figs. 23(a) and 23(b) show the UC result for MT and DE in the real sample of 100 days, respectively. As in Scenario 1, the DE is off only the last 3 hours of the day, whereas this behavior is more evenly distributed throughout the day for the MT, but always with a higher probability of being off the last 3 hours. These results are similar to those obtained previously.

Figs. 24(a) and 24(b) also show a similar trend for the simulations obtained for Scenario 2.

5.2.4. Comparative analysis for Scenario 2

Also for Scenario 2, the value of the mean value of the objective function is compared, which is equal to € 6779.6, with the result obtained in Alvarado-Barrios et al. (2020b) "case 4" (i.e. "case 4"), which is equal to € 2884.8. It seems clear that in this case, the solution is also influenced by the optimistic WT and PV scenario considered by the authors. If the simulated data are considered, the mean of the objective function is equal to € 6458.1, which is very close to the value obtained for the real data above and is lower than the mean of the objective function of the simulated data for Scenario 1 (equal to € 6841.1). For completeness and to better illustrate how optimistic the result obtained in Alvarado-Barrios et al. (2020b) is, Fig. 25 shows the histogram of the objective function of the real and simulated data with the indication of the mean value. The two distributions are very similar for both cases.

6. Conclusion

In this article, a model has been proposed to solve the scheduling problem of a hybrid generation MG, highlighting the influence
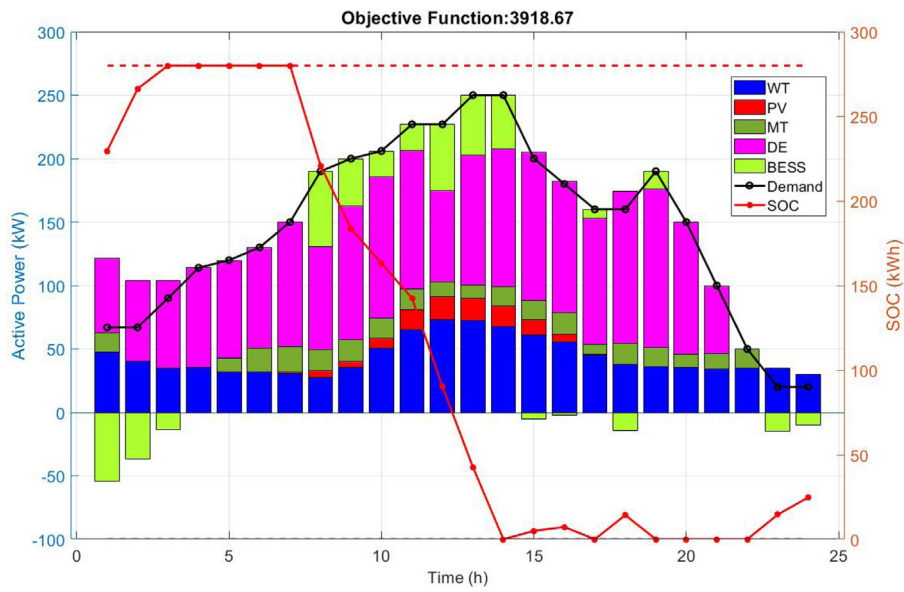
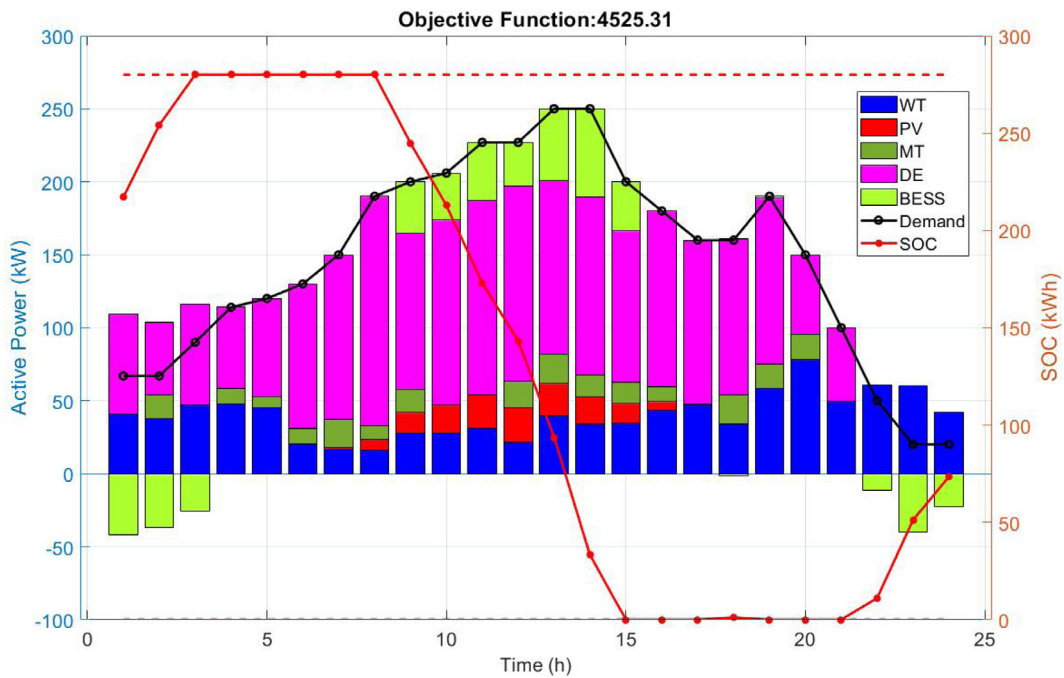**Fig. 21.** Demand coverage curve of the day 30th October in real data for Scenario 2.

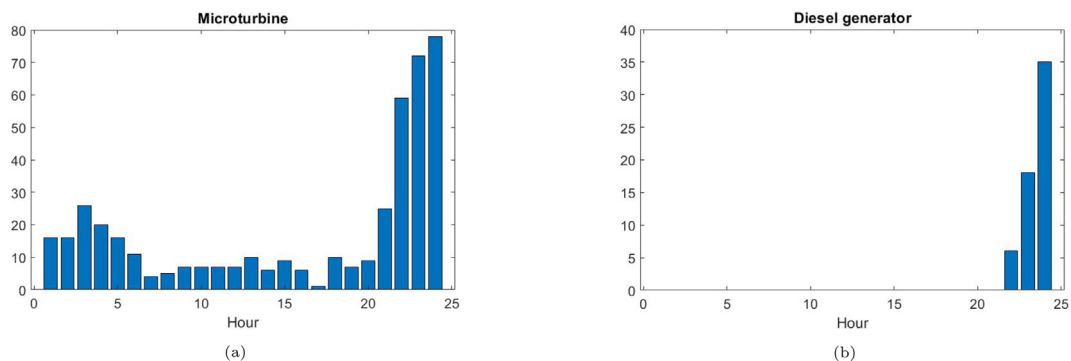**Fig. 22.** Demand coverage curve of the day 2nd November in simulated data for Scenario 2.

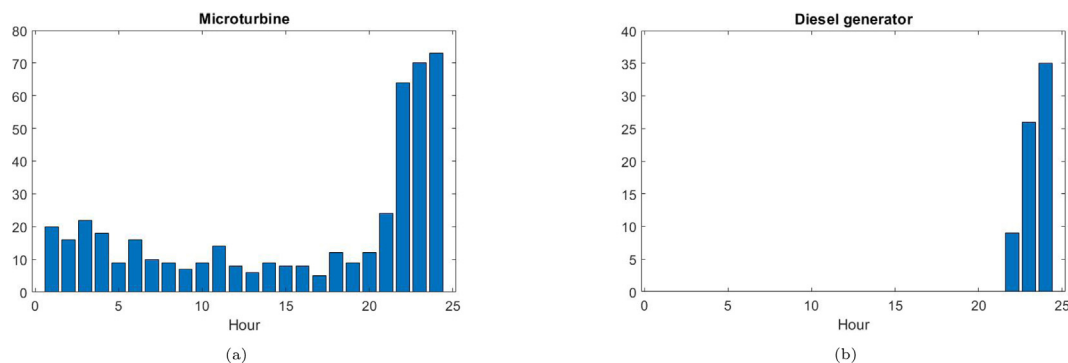**Fig. 23.** Hourly off-status histograms of MT (a) and DE (b) for the real 100-day sample for Scenario 2.

Fig. 24. Hourly off-status histograms of MT (a) and DE (b) for the simulated 100-day sample for Scenario 2.
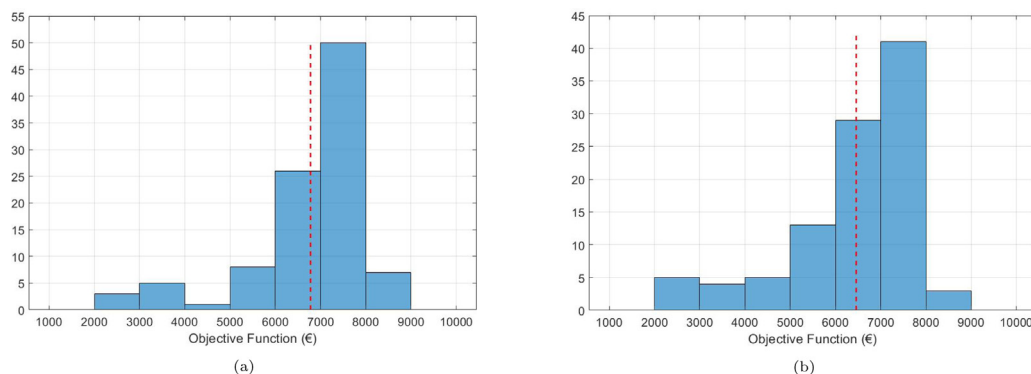

Fig. 25. Objective function histograms of real (a) and simulated (b) data with indication of the mean value for Scenario 2.

of the uncertainty of renewable energy on the final result. An SUC and an ED have been solved to schedule the management of isolated MG with the total cost as the objective function to be minimized. Demand forecasting is performed using the ARMA model, which is applied to 2 years of historical data. WT and PV productions are modeled using a non-homogeneous Markov reward process and a homogeneous Markov reward process applied to the residuals, respectively. The 100-day objective function is obtained for both real and simulated data considering the two scenarios studied. First, it is shown that the implemented stochastic models adequately simulate the behavior of the RESs, where it is evident that the total cost faced by the MG is strongly influenced by the wind speed present on each day considered. The PV power is found to influence the objective function only in terms of the general trend, which is visually translated into slopes of $6.9 \div 8.6$ for the first scenario and $7.2 \div 8.2$ for the second scenario. The slopes are positive because a time period starting from August 1st and lasting 100 days is considered and consequently corresponds to a period in which solar irradiance decreases over time. Furthermore, 50 simulations of two fixed days have been performed for each scenario to show the following two aspects: the value of the mean objective function is higher when the PV contribution is lower and the variability of the values is considerably high due to the stochasticity of the RES contributions. Due to the large amount of data processed, the UC distributions for the MT and the DE are obtained, and it is found that the highest probability of having these two devices off is in the last 3 h of the day. Compared to the study conducted in Alvarado-Barrios et al. (2020b), we want to highlight the importance of correctly considering and modeling the stochastic nature of RESs. Using the stochastic Markov model, it is shown that the WT and PV conditions considered in that study are very optimistic and do not capture the true nature of the phenomena. In the present

work, for simplification, a battery degradation model and a cost associated with the production of renewable energy have not been taken into account. These and others, such as the reduction of computational cost in the design phase and the incorporation of a physical MG to carry out frequency and voltage stability studies, are proposed as future research work along the same lines.

Declaration of competing interest

The authors declare that they have no known competing financial interests or personal relationships that could have appeared to influence the work reported in this paper.

References

Ahmadi, S.E., Rezaei, N., Khayyam, H., 2020. Energy management system of networked microgrids through optimal reliability-oriented day-ahead self-healing scheduling. Sustain. Energy, Grids Netw. 23, 100387.

Alasali, F., Haben, S., Holderbaum, W., 2019. Stochastic optimal energy management system for rtg cranes network using genetic algorithm and ensemble forecasts. J. Energy Storage 24, 100759.

Alvarado-Barrios, L., del Nozal, A.R., Valerino, J.B., Vera, I.G., Martínez-Ramos, J.L., 2020a. Stochastic unit commitment in microgrids: Influence of the load forecasting error and the availability of energy storage. Renew. Energy 146, 2060–2069.

Alvarado-Barrios, L., del Nozal, A.R., Valerino, J.B., Vera, I.G., Martínez-Ramos, J.L., 2020b. Stochastic unit commitment in microgrids: Influence of the load forecasting error and the availability of energy storage. Renew. Energy 146, 2060–2069.

Askarzadeh, A., 2018. A memory-based genetic algorithm for optimization of power generation in a microgrid. IEEE Trans. Sustain. Energy 9 (3), 1081–1089.

Atwa, Y., El-Saadany, E., Salama, M., Seethapathy, R., 2009. Optimal renewable resources mix for distribution system energy loss minimization. IEEE Trans. Power Syst. 25 (1), 360–370.

Bejan, A.I., Gibbens, R.J., Kelly, F.P., 2012. Statistical aspects of storage systems modelling in energy networks. In: 2012 46th Annual Conference on Information Sciences and Systems (Ciss). IEEE, pp. 1–6.

Bolurian, A., Akbari, H., Mousavi, S., 2022. Day-ahead optimal scheduling of microgrid with considering demand side management under uncertainty. Electr. Power Syst. Res. 209, 107965.

Bordons, C., Garcia-Torres, F., Ridao, M.A., 2020. Model Predictive Control of Microgrids. Springer.

Chen, C., Duan, S., Cai, T., Liu, B., Hu, G., 2011a. Smart energy management system for optimal microgrid economic operation. IET Renew. Power Gener. 5 (3), 258–267.

Chen, S.X., Gooi, H.B., Wang, M., 2011b. Sizing of energy storage for microgrids. IEEE Trans. Smart Grid 3 (1), 142–151.

Choudhury, S., 2022. Review of energy storage system technologies integration to microgrid: Types, control strategies, issues, and future prospects. J. Energy Storage 48, 103966.

D'amico, G., Gismondi, F., Janssen, J., Manca, R., Petroni, F., di Prignano, E., 2018. The study of basic risk processes by discrete-time non-homogeneous markov processes. Theory Probab. Math. Statist. 96, 27–43.

D'Amico, G., Petroni, F., Prattico, F., 2013. First and second order semi-markov chains for wind speed modeling. Physica A 392 (5), 1194–1201.

D'Amico, G., Petroni, F., Prattico, F., 2014. Wind speed and energy forecasting at different time scales: A nonparametric approach. Physica A 406, 59–66.

D'Amico, G., Petroni, F., Vergine, S., 2021. An analysis of a storage system for a wind farm with ramp-rate limitation. Energies 14 (13), 4066.

Eghbali, N., Hakimi, S.M., Hasankhani, A., Derakhshan, G., Abdi, B., 2022. Stochastic energy management for a renewable energy based microgrid considering battery, hydrogen storage, and demand response. Sustain. Energy, Grids Netw. 100652.

Eniola, V., Suriwong, T., Sirisamphanwong, C., Ungchittrakool, K., 2019. Hour-ahead forecasting of photovoltaic power output based on hidden markov model and genetic algorithm. International Int. J. Renew. Energy. Res 9 (2), 933–943.

Gabriel, L.G., Ruiz-Cruz, R., Zúñiga-Grajeda, V., Gurubel-Tun, K., Coronado-Mendoza, A., et al., 2022. Optimizing the penetration of standalone microgrid, incorporating demand side management as a guiding principle. Energy Rep. 8, 2712–2725.

Gast, N., Tomozei, D.-C., Le Boudec, J.-Y., 2014. Optimal generation and storage scheduling in the presence of renewable forecast uncertainties. IEEE Trans. Smart Grid 5 (3), 1328–1339.

Gerbaulet, C., von Hirschhausen, C., Kemfert, C., Lorenz, C., Oei, P.-Y., 2019. European electricity sector decarbonization under different levels of foresight. Renew. Energy 141, 973–987.

G.E.S. Data, I.S.C.G. DISC, 2015a. Global modeling and assimilation office (gmao), merra-2. last accessed 20 2021 https://disc.gsfc.nasa.gov/datasets/M2T1NXFLX_5.12.4/summary.

G.E.S. Data, I.S.C.G. DISC, 2015b. Global modeling and assimilation office (gmao), merra-2. last accessed 10 2021, https://disc.gsfc.nasa.gov/datasets/M2T1NXRAD_5.12.4/summary.

Ghasemi-Marzbali, A., Ahmadiahangar, R., Orimi, S.G., Shafiei, M., Häring, T., Rosin, A., 2021. Energy management of an isolated microgrid: A practical case. In: IECON 2021–47th Annual Conference of the IEEE Industrial Electronics Society. IEEE, pp. 1–6.

Kakran, S., Chanana, S., 2018. Smart operations of smart grids integrated with distributed generation: A review. Renew. Sustain. Energy Rev. 81, 524–535.

Khan, A.A., Naeem, M., Iqbal, M., Qaisar, S., Anpalagan, A., 2016. A compendium of optimization objectives, constraints, tools and algorithms for energy management in microgrids. Renew. Sustain. Energy Rev. 58, 1664–1683.

Kiptoo, M.K., Lotfy, M.E., Adewuyi, O.B., Conteh, A., Howlader, A.M., Senjyu, T., 2020. Integrated approach for optimal techno-economic planning for high renewable energy-based isolated microgrid considering cost of energy storage and demand response strategies. Energy Convers. Manage. 215, 112917.

Lasnier, F., Ang, T., 1990. Photovoltaic engineering handarticle.

Lei, Y., Mullane, A., Lightbody, G., Yacamini, R., 2006. Modeling of the wind turbine with a doubly fed induction generator for grid integration studies. IEEE Trans. Energy Convers. 21 (1), 257–264.

Li, Y.-z., Luan, R., Niu, J.-c., 2008. Forecast of power generation for grid-connected photovoltaic system based on grey model and markov chain. In: 2008 3rd IEEE Conference on Industrial Electronics and Applications. IEEE, pp. 1729–1733.

Li, P., Xu, D., 2014. Optimal operation of microgrid based on improved binary particle swarm optimization algorithm with double-structure coding. In: 2014 International Conference on Power System Technology. IEEE, pp. 3141–3146.

Marneris, I.G., Biskas, P.N., Bakirtzis, A.G., 2017. Stochastic and deterministic unit commitment considering uncertainty and variability reserves for high renewable integration. Energies 10 (1), 140.

Moretti, L., Martelli, E., Manzolini, G., 2020. An efficient robust optimization model for the unit commitment and dispatch of multi-energy systems and microgrids. Appl. Energy 261, 113859.

Nejat, P., Jomehzadeh, F., Taheri, M.M., Gohari, M., Majid, M.Z.A., 2015. A global review of energy consumption, CO2 emissions and policy in the residential sector (with an overview of the top ten CO2 emitting countries). Renew. Sustain. Energy Rev. 43, 843–862.

Nemati, M., Bennimar, K., Tenbohlen, S., Tao, L., Mueller, H., Braun, M., 2015. Optimization of microgrids short term operation based on an enhanced genetic algorithm. pp. 1–6.

Nikkhah, S., Nasr, M.-A., Rabiee, A., 2020. A stochastic voltage stability constrained ems for isolated microgrids in the presence of pevs using a coordinated uc-opf framework. IEEE Trans. Ind. Electron. 68 (5), 4046–4055.

O'Neill, D., Yildiz, B., Bilbao, J.I., 2022. An assessment of electric vehicles and vehicle to grid operations for residential microgrids. Energy Rep. 8, 4104–4116.

Ortega-Vazquez, M.A., Kirschen, D.S., 2007. Optimizing the spinning reserve requirements using a cost/benefit analysis. IEEE Trans. Power Syst. 22 (1), 24–33.

Papaefthymiou, G., Klockl, B., 2008. Mcmc for wind power simulation. IEEE Trans. Energy Convers. 23 (1), 234–240.

Pappas, S.S., Ekonomou, L., Karamousantas, D.C., Chatzarakis, G., Katsikas, S., Liatsis, P., 2008. Electricity demand loads modeling using autoregressive moving average (arma) models. Energy 33 (9), 1353–1360.

Pye, S., Li, P.-H., Keppo, I., O'Gallachoir, B., 2019. Technology interdependency in the United Kingdom's low carbon energy transition. Energy Strategy Rev. 24, 314–330.

Querini, P.L., Manassero, U., Fernádez, E., Chiotti, O., 2021. A two-level model to define the energy procurement contract and daily operation schedule of microgrids. Sustain. Energy, Grids Netw. 26, 100459.

Rana, M.M., Romlie, M.F., Abdullah, M.F., Uddin, M., Sarkar, M.R., 2021. A novel peak load shaving algorithm for isolated microgrid using hybrid pv-bess system. Energy 234, 121157.

Rebours, Y., Kirschen, D., 2005. What is Spinning Reserve. Vol. 174, (175), The University of Manchester.

Reddy, S., Panwar, L.K., Panigrahi, B., Kumar, R., Alsumaiti, A., 2019. Binary grey wolf optimizer models for profit based unit commitment of price-taking genco in electricity market. Swarm Evol. Comput. 44, 957–971.

Rehman, H., Reda, F., Paiho, S., Hasan, A., 2019. Towards positive energy communities at high latitudes. Energy conversion and management 196, 175–195. http://dx.doi.org/10.1016/j.enconman.2019.06.005.

REScoop.eu, 2020. Energy communities under the clean energy package transposition guidance, Transposition guidance, European federation of citizen energy cooperatives, Avenue Milcamps 103, 1030 Brussels, Belgium. https://www.rescoop.eu/toolbox/how-can-eu-member-states-support-energy-communities.

Tapia, A., Tapia, G., Ostolaza, J.X., Saenz, J.R., 2003. Modeling and control of a wind turbine driven doubly fed induction generator. IEEE Trans. Energy Convers. 18 (2), 194–204.

Thornburg, J., Krogh, B.H., 2021. A tool for assessing demand side management and operating strategies for isolated microgrids. Energy Sustain. Dev. 64, 15–24.

Tostado-Véliz, M., Kamel, S., Aymen, F., Jordehi, A.R., Jurado, F., 2022a. A stochastic-igdt model for energy management in isolated microgrids considering failures and demand response. Appl. Energy 317, 119162.

Tostado-Véliz, M., Kamel, S., Hasanien, H.M., Turky, R.A., Jurado, F., 2022b. A mixed-integer-linear-logical programming interval-based model for optimal scheduling of isolated microgrids with green hydrogen-based storage considering demand response. J. Energy Storage 48, 104028.

Trivedi, R., Patra, S., Sidqi, Y., Bowler, B., Zimmermann, F., Deconinck, G., Papaemmanouil, A., Khadem, S., 2022. Community-based microgrids: Literature review and pathways to decarbonise the local electricity network. Energies 15 (3), 918.

Wang, Z., Munawar, U., Paranjape, R., 2020. Stochastic optimization for residential demand response with unit commitment and time of use. IEEE Trans. Ind. Appl. 57 (2), 1767–1778.

Xie, P., Guerrero, J.M., Tan, S., Bazmohammadi, N., Vasquez, J.C., Mehrzadi, M., Al-Turki, Y., 2021. Optimization-based power and energy management system in shipboard microgrid: A review. IEEE Syst. J. 16, 578–590.

Yang, L., He, M., Zhang, J., Vittal, V., 2015. Support-vector-machine-enhanced markov model for short-term wind power forecast. IEEE Trans. Sustain. Energy 6 (3), 791–799.

Zia, M.F., Elbouchikhi, E., Benbouzid, M., 2018. Microgrids energy management systems: A critical review on methods, solutions, and prospects. Appl. Energy 222, 1033–1055.